

1 **Photochemistry of Methane and Ethane in the Martian**
2 **Atmosphere**

3 **Benjamin M. Taysum^{1,2} and Paul I. Palmer^{1,2}**

4 ¹School of GeoSciences, University of Edinburgh, Edinburgh, UK

5 ²Centre for Exoplanet Science, University of Edinburgh, Edinburgh, UK

6 **Key Points:**

- 7 • Formaldehyde and formic acid are two key photochemical products of CH₄ and
8 C₂H₆.
9 • Oxidation of C₂H₆ produces distinct profiles of acetaldehyde.
10 • Photolysis of acetaldehyde, produced by C₂H₆ photochemistry, is a source of at-
11 mospheric CH₄.

Corresponding author: Benjamin M. Taysum, Ben.Taysum@ed.ac.uk

Abstract

We develop an existing 1-D photochemistry model to include a comprehensive description of organic chemistry on Mars that includes the oxidation products of methane (CH_4) and ethane (C_2H_6), a longer-chain hydrocarbon that can be used to differentiate between abiotic and biotic surface releases of CH_4 . We find that CH_4 is most volatile between 20–50 km during Mars’ northern summer, where the local atmospheric CH_4 lifetime lowers to 25–60 years. We study atmospheric formaldehyde (HCHO) and formic acid (HCOOH), as the two common oxidation products of CH_4 and C_2H_6 , and acetaldehyde (CH_3CHO) and acetic acid (CH_3COOH) as unique products of C_2H_6 . We focus our analysis of these gases at Mars’ aphelion and perihelion at latitudes between -30° and 30° , altitudes from the surface to 70 km, and from a homogeneous initial condition of 50 pptv of CH_4 and C_2H_6 . From this initial condition, CH_4 produces HCHO in a latitude-independent layered structure centred at 20–30 km at aphelion with column-averaged mixing ratios of 10^{-4} pptv, and oxidation of C_2H_6 produces HCHO at 10^{-2} pptv. Formic acid has an atmospheric lifetime spanning 1–10 sols below 10 km that shows little temporal or zonal variability, and is produced in comparable abundances (10^{-5} pptv) by the oxidation of C_2H_6 and CH_4 . We also find that oxidation of 50 pptv of C_2H_6 results in 10^{-3} pptv of CH_3CHO and 10^{-4} pptv of CH_3COOH . Subsequent UV photolysis of this CH_3CHO results in 10^{-4} pptv of atmospheric CH_4 , potentially representing a new atmospheric source of Martian CH_4 .

Plain Language Summary

Reports of atmospheric methane (CH_4) on Mars, a potential biosignature, have been made via ground-based telescopes, the Mars Express orbiter, and the Curiosity Rover. However, atmospheric CH_4 has been not observed by all instruments, including the recently launched ExoMars Trace Gas Orbiter. Reconciling these different measurements of the Martian atmosphere with photochemical model calculations remains a challenge, implying that models are missing a CH_4 loss process and/or there are uncharacterised errors in the data. Here we use a photochemical model of CH_4 and ethane (C_2H_6) and their oxidation products, many of which can now be observed from orbiting satellites, to help reconcile models and data. Using this model, we show that UV photolysis of acetaldehyde, an oxidation product of C_2H_6 , is a small but potentially significant source of atmospheric CH_4 .

1 Introduction

There is considerable debate in the community about the validity and robustness of detections of atmospheric methane (CH_4) on Mars. Detections and non-detections of atmospheric CH_4 have been reported using data collected by satellites (Formisano et al., 2004; Geminale et al., 2011; Fonti & Marzo, 2010; Geminale et al., 2008; Giuranna et al., 2019), Earth-based telescopes (Mumma et al., 2009; Villanueva et al., 2013; Krasnopolsky, 2012; V. A. Krasnopolsky, 2007; Krasnopolsky, 2011; Krasnopolsky et al., 2004; V. Krasnopolsky et al., 1997) and *in situ* instruments (Webster et al., 2018, 2015; Moores et al., 2019). This debate highlights the difficulty of measuring atmospheric CH_4 on Mars, and the gaps in our current understanding of the production and loss terms that determine atmospheric CH_4 on Mars. We explore how the presence of CH_4 could be determined by its oxidation products and in the process discuss how abiotic CH_4 could be potentially produced by organic chemistry.

Detections of atmospheric CH_4 at the Gale crater by the NASA Curiosity Rover were observed episodically rising from mean volume mixing ratios (VMRs) of 0.69 ± 0.25 parts per billion (ppbv) to 7.20 ± 2.10 ppbv across a 60-sol period (Webster et al., 2015). The diurnal variations of CH_4 observations via Curiosity have recently been substantiated by the ExoMars Trace Gas Orbiter’s Nadir and Occultation for Mars Discovery (NO-

62 MAD) spectrometer and Atmospheric Chemistry Suite (ACS)(Moores et al., 2019; Ko-
63 rablev et al., 2019). These recent measurements by NOMAD and ACS constrain the up-
64 per limit of CH₄ in the Martian atmosphere to 0.05 ppbv.

65 Ground-based telescopes reported a signal of a plume that contained approximately
66 19,000 tonnes of CH₄ (Mumma et al., 2009) near the Syrtis Major region during Mars’
67 northern hemisphere’s midsummer, consistent with an estimated 0.60 kg m⁻²s⁻¹ sea-
68 sonal point source of organic compounds. Other searches for CH₄ on Mars have conversely
69 failed to detect the compound (Webster et al., 2013), including the Trace Gas Orbiter’s
70 year and a half long search(Korablev et al., 2019). This highlights the possibility of methane
71 being significantly more temporally variable than current models predict (Lefèvre & For-
72 get, 2009). This inconsistency with regards to CH₄’s detection has also ignited some polemic
73 against the existence of the gas on Mars (Zahnle et al., 2011). Recent analysis of data
74 from the Planetary Fourier Spectrometer (PFS) aboard the Mars Express orbiter iden-
75 tified the presence of CH₄ in the Martian atmosphere that was confirmed via indepen-
76 dent observations by Giuranna et al. (2019). These results appear to confirm Curiosity’s
77 detection of CH₄ at the Gale Crater. The team retrieved column integrated VMRs of
78 15.5 ± 2.50 ppbv above the Gale Crater only 1 Martian day (sol) after the Curiosity rover’s
79 measurement of a 5.78 ± 2.27 ppbv (Webster et al., 2015).

80 To further study these possible emissions of CH₄, and to also provide a more de-
81 tailed series of observations of the vertical structure and composition of Mars’ atmosphere,
82 the ExoMars mission program was established by the European Space Agency (ESA)
83 (Vago et al., 2015) and the Russian Roscosmos State Corporation for Space Activities.
84 The first mission conducted within this program was the launch of the Trace Gas Or-
85 biter (TGO) in 2016, that included two suites of spectrometers, the Nadir and Occul-
86 tation for MArS Discovery (NOMAD) spectrometer (Vandaele et al., 2018) and the At-
87 mospheric Chemistry Suite (ACS) (Korablev et al., 2017). The TGO underwent 11 months
88 of aerobraking to reduce its orbital speed and altitude, eventually establishing an approx-
89 imately circular orbit of altitude roughly 400 km allowing scientific observations to start
90 in April 2018 (Vandaele et al., 2019). Over the first year, no successful observations of
91 CH₄ were reported by the TGO instrumentation (Korablev et al., 2019). We developed
92 our investigation bearing in mind the capabilities of TGO instruments, especially the so-
93 lar occultation channels of NOMAD (NOMAD-SO) and ACS (ACS-MIR). The NOMAD-
94 SO instrument has been designed to be sensitive to CH₄ abundances as low as 0.025 ppbv
95 when observed in solar occultation mode (Robert et al., 2016). This expected detection
96 limit was compared to the experimental values in (Vandaele et al., 2019). The TGO in-
97 struments improved the experimental upper limit of previous instrumentation to reach
98 a limit of roughly 0.05 ppbv for methane. A few profiles reported in Korablev et al. (2019)
99 and obtained via ACS-MIR, measured in clear northern conditions, were able to achieve
100 the most precise detection limits of 0.012 ppbv down to an altitude of roughly 3 km.

101 Previous studies using 1-D photochemical models (Wong et al., 2003; Summers et
102 al., 2002) calculate the photochemical lifetime of CH₄ to be roughly 300 years below 70 km.
103 In the absence of a strong surface loss process, surface emissions of CH₄ will then be-
104 come homogeneously distributed across the planet after being introduced into the at-
105 mosphere. This inconsistency between models and data means that the available atmo-
106 spheric data is misinterpreted, and/or there is a loss mechanism that we do not cur-
107 rently consider in models (V. A. Krasnopolsky, 2006). Previous calculations using a global
108 3-D general circulation model have determined that to reconcile models and data we need
109 a CH₄ loss process that is up to 600 times faster than any known process (Lefèvre & For-
110 get, 2009). That additional sink would lower the atmospheric lifetime of CH₄ from cen-
111 turies to less than 200 days. With the advent of the TGO, another approach we can take
112 is to analyse observed spatial and temporal variations of the oxidation products of at-
113 mospheric CH₄.

114 In this study, we describe the development of the 1-D photochemistry submodule
 115 from the LMD-UK General Circulation Model (GCM) (Forget et al., 1999; Lewis et al.,
 116 1999) to include organic chemistry and run it as an independent model to study pho-
 117 tochemistry on Mars. We report results from a series of numerical experiments that de-
 118 scribe how the presence of CH₄ affects photochemistry on Mars. We also report pho-
 119 tochemical results when we replace CH₄ with ethane (C₂H₆) to show this longer-chain hy-
 120 drocarbon produced richer atmospheric chemistry but also allows us to consider an abi-
 121 otic source of atmospheric CH₄ from the oxidation of acetaldehyde. In the next section
 122 we describe our developed 1-D model of Mars photochemistry. In section 3 we report re-
 123 sults from our numerical experiments. We conclude the paper in section 4 in which we
 124 discuss the implications of our results for broadly understanding atmospheric chemistry
 125 on Mars but in particular the implications for detecting the presence of CH₄ and C₂H₆
 126 on Mars using their oxidation products.

127 2 1-D Photochemical Model

128 We use the 1-D photochemistry submodule from the parent 3-D LMD-UK Mars
 129 General Circulation Model as the basis for a standalone 1-D model that includes an im-
 130 proved treatment of atmospheric organic photochemistry.

131 We use this standalone 1-D model to describe time-dependent vertical distributions
 132 of trace gases from the surface to an altitude of approximately 70 km, described by 25
 133 vertical layers with a resolution of under 0.5km below 2 km increasing to a resolution
 134 of 10 km above an altitude of 20 km where 3-D macroscopic processes begin to domi-
 135 nate. We divide a Mars sol into 48 time steps ($\Delta t = 1800$ s), allowing us to describe di-
 136 urnal variations of trace gases by calculating time-dependent changes in solar zenith an-
 137 gle, taking into consideration changes in solar longitude and axial tilt. To decrease the
 138 stiffness of the discretized equations used to compute the photochemical rates of change,
 139 determined by a prescribed chemical mechanism described below, we use a chemistry sub-
 140 timestep of $\Delta t_c = 600$ s.

141 Vertical tracer transport between model layers is described by the classical diffu-
 142 sion equation (Mellor & Yamada, 1982). For details on the vertical diffusion and turbu-
 143 lent mixing routines we refer the reader to Forget et al. (1999). We use a radiative trans-
 144 fer scheme (Madeleine et al., 2011) that uses opacity values from the Mars Climate Database
 145 v5.3. We describe the condensation and sublimation of carbon dioxide, (Forget et al.,
 146 1998), water ice (Navarro et al., 2014), and hydrogen peroxide (H₂O₂); and an implicit
 147 chemistry solver computes production and loss rates from photochemical reactions.

148 2.1 Organic Photochemistry

149 The 1-D submodel that resides in the LMD-UK MGCM describes the atmospheric
 150 chemistry and transport of 15 trace gases: carbon dioxide (CO₂), carbon monoxide (CO),
 151 atomic oxygen (O), singlet oxygen (O(¹D)), molecular oxygen (O₂), ozone (O₃), hydro-
 152 gen atom (H), hydroxy radical (OH), hydroperoxyl radical (HO₂), molecular hydrogen
 153 (H₂), hydrogen peroxide (H₂O₂), nitrogen (N₂), argon (Ar), and H₂O as ice and vapour.
 154 The photochemistry scheme for these compounds consists of 32 chemical reactions (B1),
 155 and 10 photolysis reactions (B2).

156 We build on the chemical mechanism by including 41 new organic compounds, guided
 157 by previous studies (Wong et al., 2003; Summers et al., 2002) and also the theoretical
 158 measurement capabilities of the NOMAD instrument (Robert et al., 2016), to improve
 159 understanding of Mars' atmospheric chemistry. We include CH₄, C₂H₆ and its pho-
 160 tochemical products. The extended chemical mechanism represents an additional 106 chem-
 161 ical reactions (B1) and 29 photolysis reactions (B6). A complete list of trace gas species

162 within the 1-D model is provided in Table 1. We present the first analysis of C₂H₆ ox-
 163 idation products in the Martian atmosphere.

164 We take the organic chemistry rate coefficients from the CAABA/MECCA v4.0
 165 atmospheric box model (R. Sander et al., 2019), which is used to model organic chem-
 166 istry within Earth’s atmosphere. We have modified the mechanism to include HCO and
 167 C₂H₅ radicals. The CAABA/MECCA v4.0 model neglects these radicals as products,
 168 and instead includes the products of the radicals with molecular oxygen, O₂. This ap-
 169 proximation is sufficient for Earth, where O₂ is present at 21% mass fraction, but on Mars
 170 it is present only at a mass fraction of 10⁻³. Including these radicals allows us to im-
 171 prove the description of organic chemistry. All three-body reaction rate coefficients in
 172 the submodule are multiplied by a factor of 2.5, following Nair et al. (1994), to account
 173 for the increase in efficiency that CO₂ displays when used as a bath gas in comparison
 174 to N₂ or dry air (Kaufman & Kelso, 1967), commonly used in laboratories for the cal-
 175 culation of these coefficients.

176 To improve the accuracy of the original chemistry routine and to reduce the com-
 177 putational expediency of our chemistry calculation we use a pre-calculated look-up ta-
 178 ble to interpolate photolytic frequencies. We calculated these photolysis loss rates us-
 179 ing the Tropospheric Ultraviolet and Visible (TUV) Radiation Model (Madronich et al.,
 180 2002) that has been adapted for use on Mars (Lefèvre et al., 2004), and using routines
 181 to interpolate as function of atmospheric temperature, solar zenith angle, O₃ column den-
 182 sity, the total atmospheric column density, the Sun-Mars distance, and the dust opac-
 183 ity. The photolytic reaction $j_{\text{HOCH}_2\text{OOH}}$ of B6 requires the consideration of the abun-
 184 dance of O₂, as the photolytic product of HOCH₂OOH is the highly reactive HOCH₂O
 185 radical. HOCH₂O proceeds to react with molecular oxygen to form HCOOH and OH.
 186 To limit the number of compounds that the steady-state approximation has to be ap-
 187 plied to, the 1-D model multiplies the photolytic frequency extracted from the TUV look-
 188 up table by a temperature independent factor of 3.50×10^{-14} (Veyret et al., 1982) and
 189 the number density of O₂ at the respective layer.

190 To improve the accuracy of the original chemistry routine and to reduce the stiff-
 191 ness of the chemistry calculations, we decreased the chemical timestep to 600 seconds.
 192 This has the additional benefit of allowing the Semi-Implicit Backward Euler Method
 193 (SIBEM) to be used for a larger number of species across timestep Δt_c while conserv-
 194 ing mass of the studied tracers. For species with photochemical lifetimes shorter than
 195 100 seconds we consider a family of species, e.g. odd-hydrogen (HO_x) and odd-oxygen
 196 (O_x) families, which have a collective lifetime longer than the timestep. We handle these
 197 compounds, H, OH, HO₂ and O(¹D), O(³P), O₃ respectively via the assumption of pho-
 198 tochemical equilibrium (Rodrigo et al., 1990). The routine calculates dimensionless par-
 199 tition functions of the loss rates of H/HO₂, OH/HO₂, and O(³P)/O₃ (s⁻¹/s⁻¹), and sums
 200 the abundances of each family, HO_x and O_x, which possess atmospheric lifetimes greater
 201 than that of the chemistry timestep, allowing them to be computed via the SIBEM equa-
 202 tion. The partition functions are then applied to compute each individual compounds
 203 respective abundance.

204 2.2 Time-dependent meteorological boundary conditions

205 To drive the 1-D photochemistry model, we use time-dependent lateral atmospheric
 206 boundary conditions of temperature, wind, water vapour volume mixing ratios, and sur-
 207 face pressure from the Mars Climate Database v5.3 (MCD) (Millour et al., 2017). We
 208 interpolate the 3-D meteorological fields from the MCD dataset, taking into account lat-
 209 itude, solar longitude, and local time.

210 All interpolated values from the MCD dataset are longitudinal means, calculated
 211 independently by ourselves, acknowledging that there are only small longitudinal vari-
 212 ations of meteorological parameters that are due primarily to topographical features. We

Table 1. Trace gas species handled by the 1-D photochemistry submodule.

Formula	Name
Inorganic Tracers	
CO_2	Carbon Dioxide
CO	Carbon Monoxide
$O(^1D)$	Atomic Oxygen (excited singlet)
$O \equiv O(^3P)$	Atomic Oxygen (ground-state)
O_2	Molecular Oxygen
O_3	Ozone
H	Atomic Hydrogen
OH	Hydroxyl
HO_2	Hydroperoxyl
H_2O_2	Hydrogen Peroxide
H_2	Molecular Hydrogen
H_2O (vapour and ice)	Water Vapour and Ice
N_2	Nitrogen
Ar	Argon
Organic Tracers (Methane Oxidation)	
CH_4	Methane
CH_3	Methyl Radical
CH_3O_2	Methyl Peroxy-radical
CH_3OOH	Methyl Hydroperoxide
CH_3OH	Methanol
CH_3O	Methoxide
HCHO	Formaldehyde
HCOOH	Formic Acid
$HOCH_2O_2$	Hydromethyl Peroxy
$HOCH_2OH$	Methanediol
$HOCH_2OOH$	Hydromethyl Hydroperoxide
HCO	Formyl Radical
Organic Tracers (Ethane Oxidation)	
C_2H_6	Ethane
C_2H_5	Ethyl Radical
$C_2H_5O_2$	Ethyldioxy Radical
C_2H_5OOH	Ethyl Peroxide
C_2H_5OH	Ethanol
$HOCH_2CH_2O_2$	-
$HOCH_2CH_2O$	-
Ethgly ($(CH_2OH)_2$)	Ethylene Glycol
Hyetho2h ($C_2H_6O_3$)	-
CH_3CHO	Acetaldehyde
CH_2CHOH	Ethenol
CH_3CHOHO_2	Hydroxy Ethyl Peroxy Radical
CH_3COOH	Acetic Acid
$CH_3CHOHOOH$	-
$CH_3C(O)$	Acetyl Radical
$CH_3C(O)OO$	-
$CH_3C(O)OOH$	Peracetic Acid
$HCOCH_2O_2$	-
Glyox ($OCHCHO$)	Glyoxal
HCOCO	-
$HOCH_2CHO$	Hydroperoxy Acetaldehyde
$HOCH_2CHO$	Glycolaldehyde
$HOCHCHO$	Hydroxyl-Vinoy Radical
$HOCH_2CO$	-
$HOCH_2CO_3$	-
$HOCH_2CO_2H$	Glycolic Acid
$HCOCO_2H$	-
$HCOCO_3H$	-
$HCOCO_3$	-
$HOCH_2CO_3H$	-

213 take advantage of this so that the horizontal footprint of our model is representative of
 214 a zonal band of 3.75° in latitude, which is the latitudinal resolution of the MCD dataset.
 215 Zonal and meridional transport is not accounted for by the 1-D model. We use an in-
 216 terpolation routine for trace gases that have atmospheric chemistry lifetimes greater than
 217 the e-folding residence times associated with meridional advection of trace gases out of
 218 the zonal band, which is approximately 0.5–2 sols. We use this approach to drive the model
 219 with vertical profiles of CO_2 , CO , O_2 , H_2 , and water vapour, ensuring the photochem-
 220 ical environment is consistent with the meteorological fields from the MCD, allowing the
 221 1-D model to be accurately representative of the temporally and spatially variable ox-
 222 idising environment. Seasonal water vapour profiles from MCD are especially important
 223 for the 1-D photochemical calculations as the photolysis of Martian H_2O is the source
 224 of the highly reactive odd-hydrogen species, $\text{HO}_x = \text{H} + \text{OH} + \text{HO}_2$, which help drive
 225 the oxidation of organic species and O_3 chemistry (Lefèvre et al., 2004).

226 The overarching purpose of using these boundary conditions is that we can describe
 227 detailed 1-D atmospheric chemistry, including diurnal and seasonal changes associated
 228 with Mars’ atmosphere, without the computational overhead of solving the 3-D dynam-
 229 ical equations. In particular, the boundary conditions help to maintain realistic values
 230 and variations of wind profiles that underpin vertical diffusion calculations that corre-
 231 spond to calculating vertical transport. For all of our calculations, we use a prescribed
 232 dust scenario produced from the assimilation of observations of the dust optical depth
 233 made by the Mars Global Surveyor’s Thermal Emission Spectrometer (Montabone et al.,
 234 2015) during Mars Year (MY) 24. This scenario is regarded as a ‘best guess’ of the mean
 235 annual dust variability experienced on Mars without the presence of global or significant
 236 regional dust storms. The 1-D photochemical model is capable of operating in dust-storm
 237 scenarios using data from the MCD v5.3, but these calculations are beyond the scope
 238 of the current study.

239 We limit our calculations to latitudes less than 30° , where most recent observations
 240 of CH_4 on Mars have been reported (Mumma et al., 2009; Webster et al., 2018, 2015).
 241 At latitudes higher than 40° in both hemispheres, the MCD boundary conditions also
 242 allow us to describe the large-scale seasonal changes in atmospheric temperature that
 243 result from condensation, deposition and sublimation of CO_2 , which produce significant
 244 changes in surface pressure. However, at these latitudes meridional wind profiles above
 245 the planetary boundary layer can become large enough to lower the tracer e-folding timescales
 246 to values too small for the 1-D model to neglect while still producing reliable model re-
 247 sults. At latitudes less than 30° , the 1-D model in this work can be used to produce time-
 248 dependent tracer profiles for periods limited to 2 sols.

249 **2.3 Definition of Numerical Experiments**

250 We use the 1-D model to determine vertical profiles of organic compounds that evolve
 251 from a hypothetically fixed and vertically uniform 50 pptv profile of CH_4 . We have cho-
 252 sen this value because it is consistent with the upper limit of Martian CH_4 determined
 253 by data collected from the ACS/NOMAD instruments aboard the TGO (Korablev et
 254 al., 2019).

255 For this calculation, we initialise the model 10 sols prior to the point where solar
 256 longitude $L_S = 0^\circ$ with initial meteorological conditions and tracer profiles of CO_2 , CO ,
 257 O_2 , water vapour, and H_2 from the previously detailed MCD v5.3 look-up table, and 10
 258 ppbv of CH_4 distributed evenly across all 25 atmospheric layers ranging from the sur-
 259 face to approximately 70 km. We then run the 1-D over one Mars year, 668 sols, follow-
 260 ing a 10 sol spin-up period, taking into account diurnal and seasonal (orbital) variations
 261 in solar zenith angle and corresponding changes in solar flux and photolytic frequencies.
 262 We report calculations at latitudes of 30°N , 2.5°N , and 30°S to investigate possible spa-
 263 tial variations in organic product profiles.

264 Following this investigation into the annual variations of the products produced by
 265 the steady and homogeneous CH₄ background, we use the 1-D model to investigate time-
 266 dependent photochemical processes that result from oxidation of CH₄ and C₂H₆. For
 267 these experiments, we initialise the 1-D model at the required latitude and solar longi-
 268 tude at 00:00 local time (LT) with 0 pptv CH₄ and other non-methane organic compounds.
 269 We use a five-day spin-up period at a constant solar longitude when we use trace gas pro-
 270 files of CO₂, CO, O₂, H₂, and water vapour from the MCD v5.3 (section 2.2) and diurnally-
 271 varying atmospheric parameters. This spin-up enables the HO_x and O_x chemistry to par-
 272 tition to the solar-longitude environment. After five sols, we add a vertically-uniform 50 pptv
 273 profile of CH₄ at 00:00 LT. We then let the model run freely for one further sol, and present
 274 the photochemical products at a local time of 18:00 LT when solar occultation measure-
 275 ments are typically collected. We adopt a similar approach to examine the photochem-
 276 istry of C₂H₆.

277 3 Results

278 We use the 1-D model described in the previous section to understand the seasonal
 279 chemical composition of the Martian atmosphere as a function of latitude that corresponds
 280 to a fixed, uniform vertical distribution of atmospheric CH₄. We present a similar set
 281 of calculations that correspond to a uniform vertical distribution of atmospheric C₂H₆.

282 3.1 Methane Oxidation in the Atmosphere of Mars

283 Figure 1 describes the initial photochemical oxidation steps of atmospheric CH₄
 284 on Mars. The dominant atmospheric losses of CH₄ are oxidation by the hydroxyl rad-
 285 ical (OH) and the excited singlet oxygen (O(¹D))), and photolysis. The loss rates for at-
 286 mospheric CH₄ vary as a function of solar longitude. There are a number of high-yield
 287 oxidation products that are produced rapidly, potentially allowing us to colocate elevated
 288 values with CH₄ emissions, and that are observable from orbiting instruments. In this
 289 paper we will restrict our analysis to the production of formaldehyde (HCHO) and formic
 290 acid (HCOOH).

291 Figure 2 shows an illustrative vertical distribution of CH₄ loss factors (s⁻¹) at the
 292 solar longitudes of 71° and 271°, times at which Mars' orbit is furthest from and clos-
 293 est to the Sun, respectively. Loss factors, units of s⁻¹, are distinguished from loss rates,
 294 units of molec cm⁻³s⁻¹, as loss factors provide a better insight into the reactivity of the
 295 surrounding environment. These values after being multiplied by CH₄ number densities
 296 equate to the rate of photochemical loss of CH₄ (molec cm⁻³s⁻¹), i.e. the loss rate.

297 From the Martian surface to the top of the Martian hygropause, approximately 10 km
 298 at L_S 71° and 45 km at L_S 251°, the dominant loss process for CH₄ is from oxidation by
 299 OH. Consequently, at these altitudes the rate of OH production, driven by the photol-
 300 ysis of water vapour, are larger than outside this altitude range. Above these altitudes,
 301 the abundance of O(¹D) increases, reflecting the drop in its loss from reaction with wa-
 302 ter vapour. Between the top of the hygropause and roughly 60 km, O(¹D) becomes the
 303 dominant loss of atmospheric CH₄. There are three oxidation channels associated with
 304 this reaction (B4), the most efficient producing CH₃ and OH. Photolysis of CH₄ becomes
 305 significant only at altitudes higher than 60 km. The decreasing abundance of O(¹D) atoms
 306 in the upper atmosphere results in a small vertical region, 50–60 km, where CH₄ loss rates
 307 decline before photolysis becomes important at higher altitudes. Below 60 km, the ef-
 308 fect of UV radiation on CH₄ is negligible, and photochemical contributions made by methyl
 309 radical isotopologues can be disregarded. This highlights that the primary atmospheric
 310 sinks of CH₄ change seasonally, with O(¹D) dominating in the aphelion seasons, and OH
 311 dominating in the perihelion. The stronger reaction rates of O(¹D) with CH₄ can thus
 312 be expected to produce greater abundances of potentially observable organic species within
 313 the aphelion seasons of Mars.

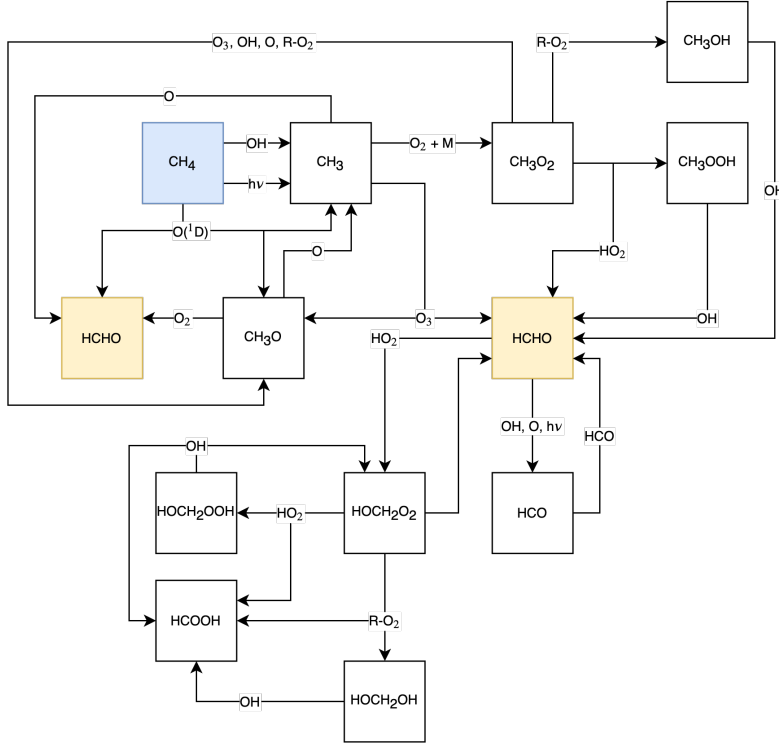


Figure 1. Primary stages of the CH_4 photochemistry that we use in our 1-D photochemistry model, taken from the CAABA/MECCA v4.0 chemical mechanism.

314 The local atmospheric lifetime of CH_4 , incorporating all chemical loss terms (Fig-
 315 ure 2), varies as a function of latitude and solar longitude. Differences between latitudes
 316 are determined by the solar radiation being received, which is a function of solar longi-
 317 tude and Mars' obliquity. Local atmospheric lifetimes range from 25 to 1700 years (Ap-
 318 pendix A1). These values, with a significant and localized surface loss process, would gen-
 319 erate a large, slowly varying background value for CH_4 that would be difficult to attribute
 320 to individual surface sources. Local atmospheric lifetimes reach a minimum of 25–200
 321 years between the top of the hygropause and approximately 50 km due to the larger abun-
 322 dance of the $\text{O}(^1\text{D})$ atom. Below the hygropause where OH is the dominant sink, local
 323 atmospheric lifetimes vary between 200 and 425 years. The longest local lifetimes of 1000–
 324 1700 years lie between 50 and 60 km during winter ($L_S = 270\text{--}360^\circ$), as described above,
 325 where the OH and $\text{O}(^1\text{D})$ loss processes decline and before photolysis dominates above
 326 60 km.

327 These local atmospheric photochemical lifetimes are significantly longer than the
 328 corresponding atmospheric transport timescales across all altitudes and solar longitudes.
 329 We study the variance of these local photochemical lifetimes with solar longitude, alti-
 330 tude, and Mars latitude to understand where are the most photochemically active re-
 331 gions for CH_4 (and below for C_2H_6) and consequently where we expect the largest pro-
 332 duction rates for their oxidation products. Calculating the vertically integrated photo-
 333 chemical lifetime of CH_4 with the 1-D model (Appendix A1) yields timescales that cor-
 334 respond well to those calculated in previous studies (Lefèvre & Forget, 2009; Krasnopol-
 335 sky et al., 2004; Summers et al., 2002), with the 1-D model producing values ranging be-
 336 tween 250–550 terrestrial years across the latitude ranges studied here of 30° south to
 337 30° north.

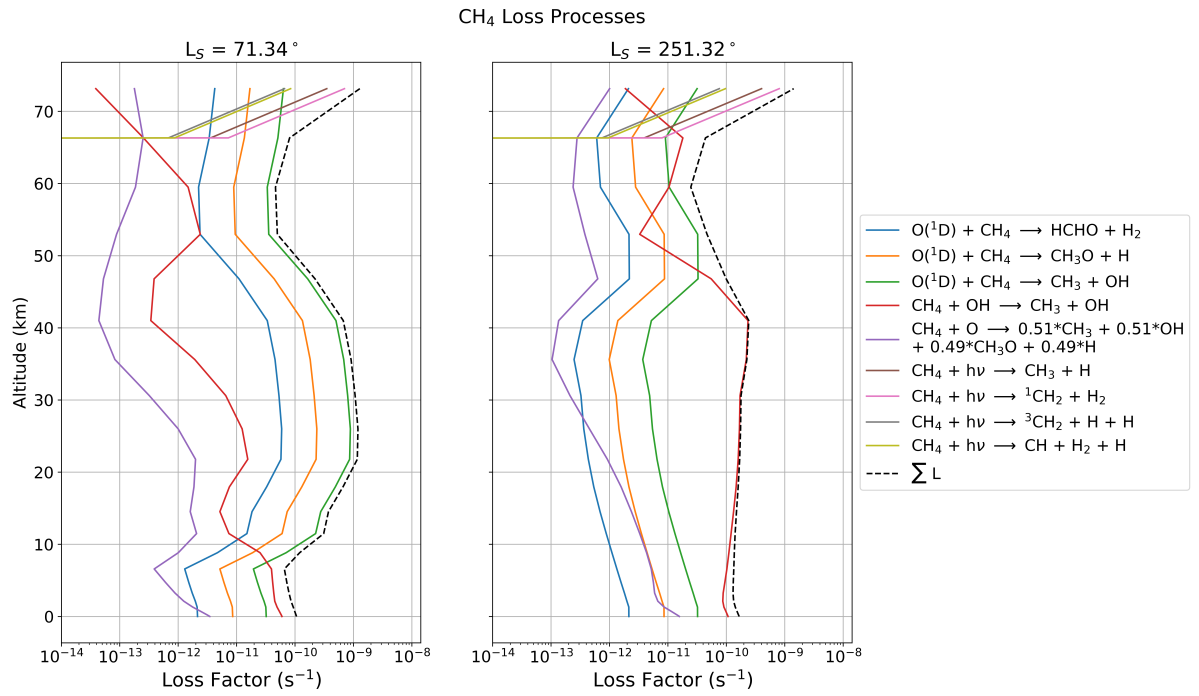


Figure 2. Photochemical loss factors (s^{-1}) CH₄ in our 1-D photochemistry model at latitude 2.5°N, local time 12:00, and solar longitudes 71° and 251° (Mars' aphelion and perihelion, respectively) as a function of altitude.

338 Figure 3 shows vertical profiles of the volume mixing ratios of organic compounds,
 339 radicals, peroxy-radicals, and long-lived species from left to right, that result from the
 340 oxidation of a fixed, uniformly distribution 50 pptv of atmospheric CH₄. For this cal-
 341 culation we initialise the 1-D model with 0 pptv of CH₄ across all vertical layers at L_S
 342 = 71° and L_S = 251°, 00:00 LT, at a latitude of 2.5°, the latitude at which a CH₄ plume
 343 has been previously observed (Mumma et al., 2009). We spin-up for five sols using de-
 344 tailed MCD v5.3 tracer profiles (section 2). We then insert a fixed, uniform profile of 50 pptv
 345 of CH₄ into the model and run forward for one sol. We sample the model at 18:00 LT
 346 on sol 6, allowing sufficient time (18 hours) for products to be produced but a short enough
 347 time to ensure these products are not advected out of the column. This allows us to study
 348 the resulting CH₄ oxidation product concentrations. We show values for CH₄, HCHO,
 349 HCOOH, methanol, methyl hydroperoxide (CH₃OOH), hydromethyl peroxy (HOCH₂O₂),
 350 and hydromethyl hydroperoxide (HOCH₂OOH). The two products with the highest pho-
 351 tochemical yields are HCHO and HCOOH. We find that HCHO has column averaged
 352 mixing ratios of 5.43×10^{-16} and 7.41×10^{-17} molecule/molecule at L_S = 71° and 251°,
 353 respectively. HCOOH has a column averaged mixing ratio of 2.31×10^{-17} and 2.08×10^{-17}
 354 molecule/molecule at L_S = 71° and 251°, respectively. We describe below the respon-
 355 sible production and loss rates associated with these two compounds.

356 Production rates of methanol are small in our 1-D model, which is driven by a re-
 357 alistic 50 pptv of CH₄. Previous studies that have used a much larger 100 ppmv profile
 358 of CH₄ (e.g. (Wong et al., 2003)) have still struggled to produce Martian methanol above
 359 pptv values. CH₃OH has prominent features at IR wavelengths, making it a valuable ob-
 360 served species to help constrain our understanding of organic chemistry. Our 1-D model
 361 calculates CH₃OH column average mixing ratios of 2.09×10^{-19} and 1.01×10^{-18} molecule/molecule
 362 at L_S = 71° and 251°, respectively. These small quantities are due to the two main pro-
 363 duction terms for CH₃OH (Table B4) involving CH₃O₂ and CH₃ radicals that are not
 364 produced in large quantities by 50 pptv of CH₄. Consequently, we will only discuss CH₃OH
 365 in context of HCHO and HCOOH.

366 3.2 Production of Formaldehyde from CH₄ Oxidation

367 HCHO is a high-yield oxidation product of CH₄ on Mars that is observable by the
 368 NOMAD and ACS spectrometers aboard the Trace Gas Orbiter. Figure 4 shows verti-
 369 cal distributions of HCHO volume mixing ratios, corresponding to a fixed vertical pro-
 370 file of 50 pptv CH₄, at 18:00 LT over all solar longitudes to determine when we might
 371 expect HCHO to be observable during one Martian year. HCHO production peaks dur-
 372 ing spring months when there is sufficient production of O(¹D) in the middle atmosphere
 373 to oxidize CH₄ but not water vapour in the lower atmosphere. We find only small vari-
 374 ations in the HCHO produced across the three latitudes, where HCHO consistently re-
 375 mains below 10⁻³ pptv. This lies well below the expected detection limit of 30–40 pptv
 376 for the TGO NOMAD instrument (Robert et al., 2016) and of 0.17–1.70 ppbv for the
 377 TGO ACS instrument (Korablev et al., 2017).

378 Figure 5 shows individual and net production and loss rates of HCHO as a func-
 379 tion of altitude at 06:30 LT, L_S = 71°, and latitude 2.5°N. We find net production peaks
 380 at 06:30 LT as the Sun begins to rise above the horizon. Figure 5a shows two distinct
 381 regions where HCHO production peaks. Below the hygropause, at roughly 15 km at this
 382 L_S, reaction between water vapour and excited atomic oxygen result in HCHO produc-
 383 tion dominated by the reaction of CH₃O₂ and HO₂. Above the hygropause at 15 km,
 384 the HCHO production is from atomic oxygen reacting with methyl and methoxy rad-
 385 icals. Figure 5b show the HCHO loss rates. We find that HCHO is lost rapidly by pho-
 386 tolysis through the atmospheric column. Below the hygropause, HCHO is lost by reac-
 387 tion with HO₂ which produced the HOCH₂O₂ peroxy radical. Above the hygropause,
 388 the dominant HCHO sink is reaction with atomic oxygen. At solar zenith angles between
 389 60 and 85°, abundances of O(³P), CH₃, and CH₃O radicals are in large enough at the

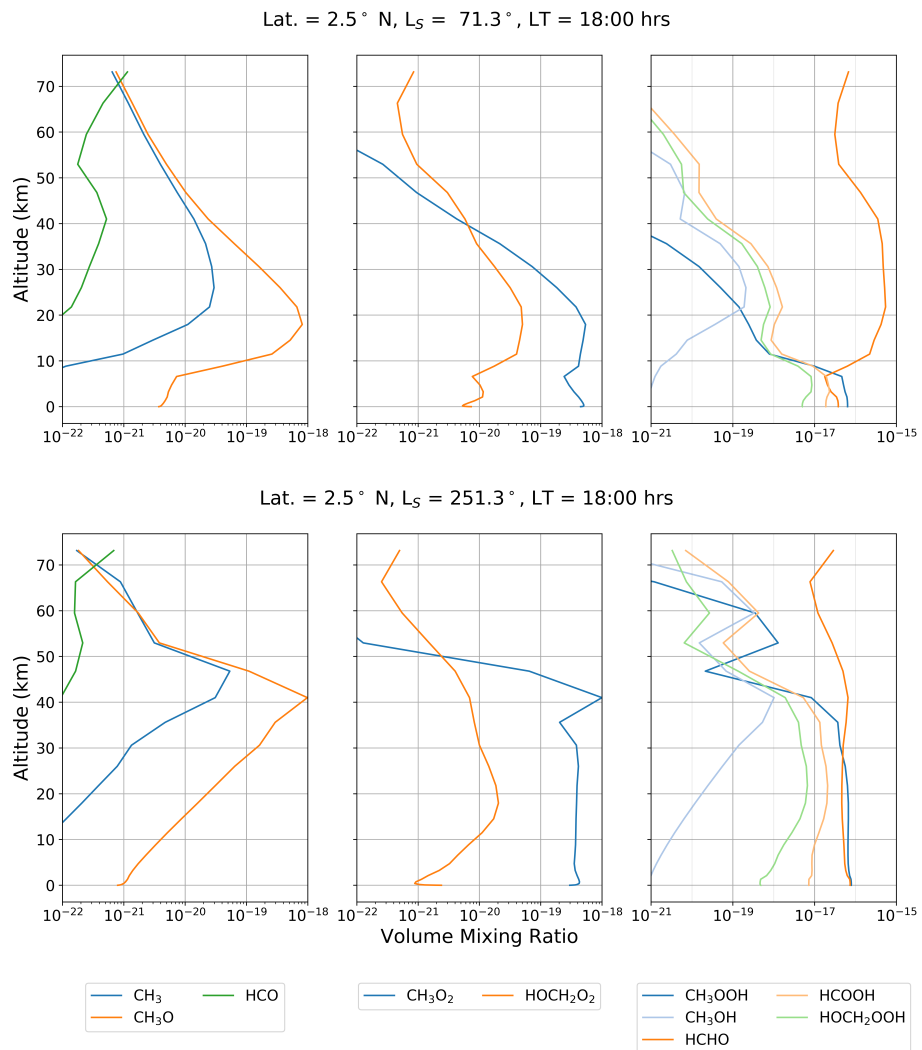


Figure 3. Volume mixing ratio profiles of major photochemical products of 50 pptv of CH₄ after one sol. These include formaldehyde (HCHO), formic acid (HCOOH), methanol (CH₃OH), methyl hydroperoxide (CH₃OOH), hydromethyl peroxy (HOCH₂O₂), and hydromethyl hydroperoxide (HOCH₂OOH).

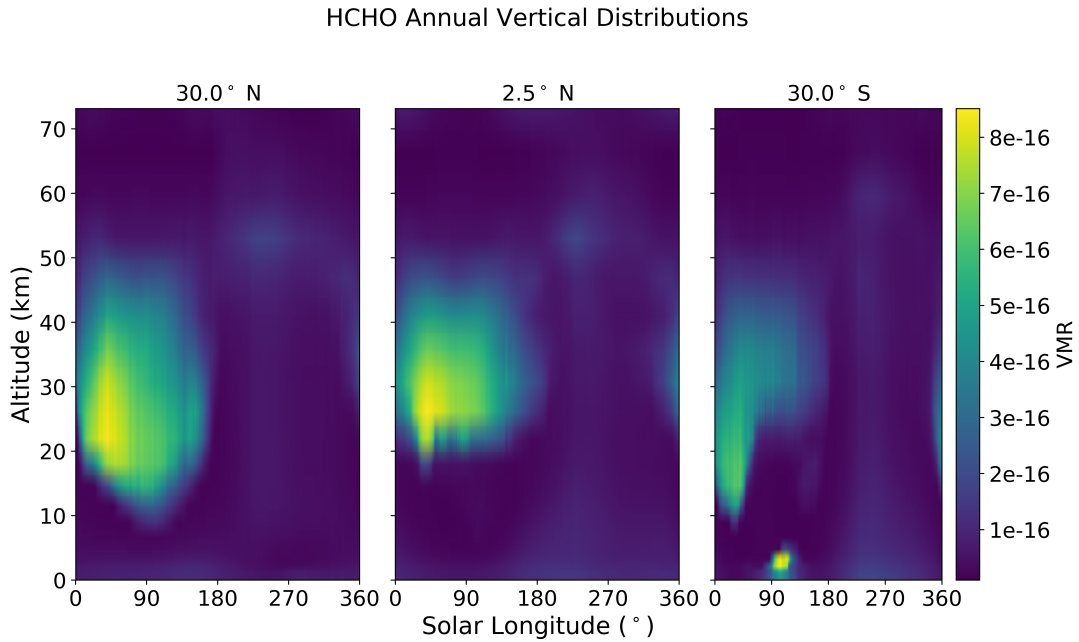


Figure 4. Vertical profiles of HCHO (pptv) from the photochemistry of 50 pptv CH₄ within a zonal band centered on latitudes 30°N, 2.5°N, and 30°S, across all solar longitudes, as calculated by our 1-D photochemical model.

390 top of the hygropause to overcome the loss of HCHO from photolysis. At lower solar zenith
 391 angles, the rate of formaldehyde photolysis is too great to allow significant net produc-
 392 tion.

393 The resulting atmospheric lifetime of HCHO for all Martian seasons is 2–6 hours
 394 at latitudes less than 30° (Appendix A2), consistent with previously published results
 395 (Wong et al., 2003). As a result, a detection of HCHO below 70 km in the Martian at-
 396 mosphere will require a strong active release of CH₄ in the local vicinity. Our calcula-
 397 tions suggest that HCHO will be most likely detected at mid-altitudes (15–30 km) across
 398 the tropics during Mars northern spring and summer months. This is due to the lower
 399 abundance of water vapor and the increased levels of odd-oxygen species available for
 400 reactions with organic radicals, and also coincides with the altitude regions where the
 401 TGO instruments are expected to display the greatest level of sensitivity (Korablev et
 402 al., 2017).

403 Using 1-D steady-state model driven by a profile of 100 ppmv CH₄, (Wong et al.,
 404 2003) report an increase in HCHO above 50 km. Our 1-D calculations are time-dependent,
 405 driven by a more realistic CH₄ value (published since (Wong et al., 2003)), and by in-
 406 terpolated atmospheric parameters that include optical opacity and long-lived inorganic
 407 tracers from a 3-D dataset. As such, we believe our approach provides a more compre-
 408 hensive and realistic modelling environment to describe atmospheric photochemistry on
 409 Mars. The photolysis loss rates for HCHO in our model at latitude 2.5° are compara-
 410 ble to those used by (Wong et al., 2003). Differences between our calculations and those
 411 reported by (Wong et al., 2003) are mainly due to smaller quantities of radicals produced
 412 by a much lower assumed value of atmospheric CH₄, and our consideration of longitu-
 413 dinal mean variations of atmospheric parameters instead of using global mean param-
 414 eters.

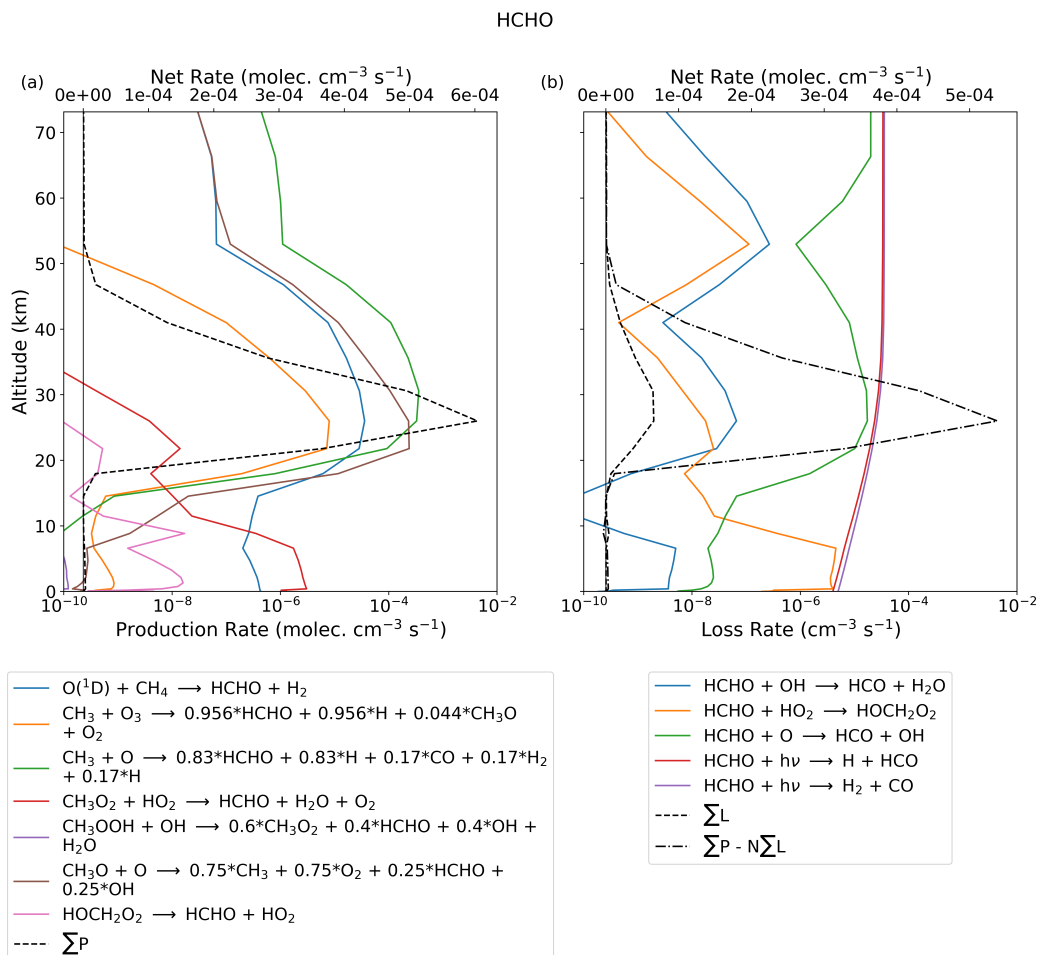


Figure 5. Photochemical production and loss rates for HCHO (molec cm⁻³s⁻¹), associated with CH₄ photochemistry, as a function of altitude. Calculations are for L_S = 71°, 06:30 LT, and latitude 2.5°N.

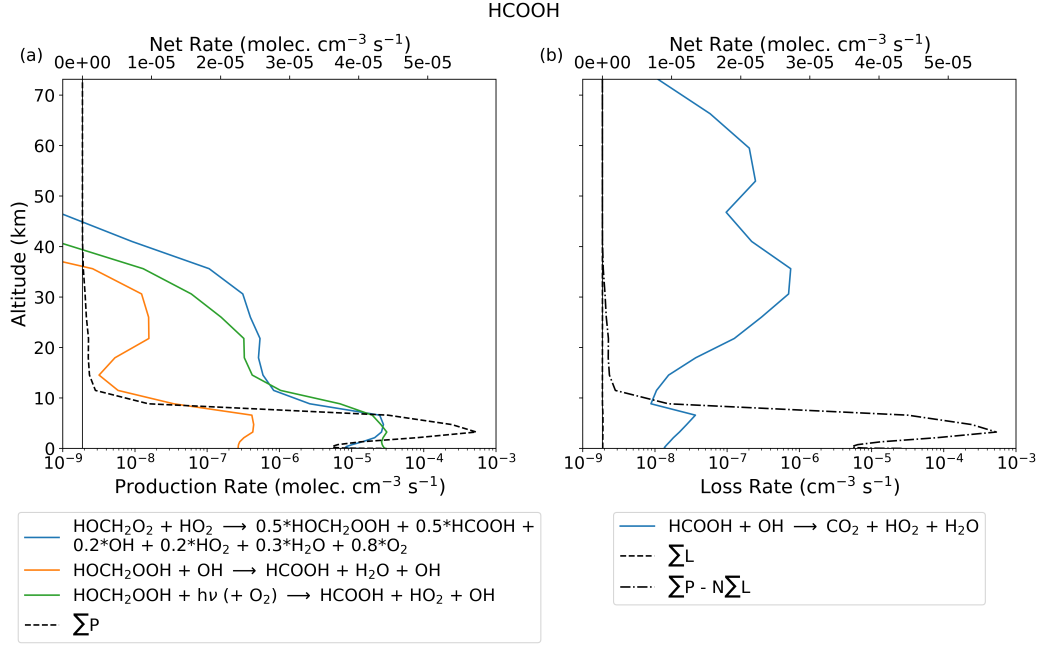


Figure 6. As Figure 5 but for formic acid (HCOOH).

415

3.3 Production of Formic Acid from CH₄ Oxidation

416

417

418

419

420

421

422

423

424

425

426

427

428

429

430

The oxidation of HCHO via HO₂ radicals leads to pathways that produce HCOOH (Figure 1). HCHO reacts with HO₂ to produce the HOCH₂O₂ peroxy radical, which can either decay into its original reactants, or react with HO₂ to produce HCOOH directly or to produce hydroxymethyl hydroperoxide that subsequently reacts with OH to produce formic acid or HOCH₂O₂, with a branching ratio, $k_{\text{HOCH}_2\text{O}_2}/k_{\text{HCOOH}}$, of 0.233 at 298 K. HOCH₂OOH can also photolyse under UV radiation to produce HOCH₂O and OH. The HOCH₂O radical proceeds to react with molecular oxygen to produce formic acid and HO₂. The only sink of HCOOH in the Martian atmosphere is via oxidation by OH. This reaction is slow, and limits loss of HCOOH to regions below the point of the hygropause. In regions where OH concentrations are at a maximum, typically during L_S = 150–340° at the top of the water vapour saturation point, HCOOH has a photochemical lifetime that range between 1 and 10 sols. From the surface to roughly 8 km, values range between 70 sols and 220 sols throughout the year in the northern hemisphere, but values in the south increase to magnitudes of 10³ sols during the northern summer (L_S = 90–180° with the lower abundances of atmospheric H₂O).

431

432

433

434

435

436

437

438

439

Figure 6 shows the net and individual production and loss rates for HCOOH for L_S = 71°, latitude 2.5°N, and LT = 18:00 due to a fixed, uniformly distribution of 50 pptv CH₄. The largest production rate of HCOOH is from HOCH₂O₂ reacting with HO₂ and from the photolysis of HOCH₂OOH. The loss of HCOOH from OH oxidation is slow compared to the production rates. Our calculations therefore suggest that a detection of HCOOH would be related to the photochemical loss of HCHO. The resulting atmospheric lifetime of HCOOH is temporally and spatially variant, with lows of 2–5 sols at the tip of the hygropause, increasing to 75–100 sols closer to the surface where the abundances of OH fall.

440

3.4 Ethane Oxidation

441

442

443

444

445

446

447

Here we consider the impact of C_2H_6 on Mars' photochemistry. The impetus for these calculations is that on Earth, emissions of CH_4 are accompanied by emissions of higher-chain hydrocarbon such as C_2H_6 (Horita & Berndt, 1999; Guenther et al., 2000). C_2H_6 is also listed as an observable compound through the NOMAD-SO and ACS-MIR instrument, with detection limits between 0.02 and 0.03 ppbv (Vandaele et al., 2018) and 0.06–6 ppbv (Korablev et al., 2017). Current knowledge puts an upper limit of 0.20 ppbv on C_2H_6 (Krasnopolsky, 2012; Villanueva et al., 2013).

448

449

450

451

452

453

Figure 7 shows that the photochemistry for C_2H_6 is more complicated than for CH_4 (B4), but follows the same general routes. It is oxidized by OH and $O(^1D)$ that initiates a series of chemical reactions that result in high yield products of HCHO and HCOOH among other compounds. One of the initial C_2H_6 oxidation product is the C_2H_5 radical, which is not described explicitly by the CAABA mechanism. We have used independent sources for reaction rates that involve the C_2H_5 radical (B5).

454

455

456

457

458

459

460

461

462

463

Figure 8 shows the photochemical loss factors for C_2H_6 in the Martian atmosphere at noon, L_S 71° and 251° , and at latitude $2.5^\circ N$. Our photolysis calculations, based on values from the TUV model (Madronich et al., 2002) and adjusted for the Sun–Mars distance, suggest this loss process is insignificant below 70 km. Similar to CH_4 , below the Martian hygropause OH is the dominant loss process for C_2H_6 , and above the hygropause $O(^3P)$ is the dominant loss process for C_2H_6 , with the $C_2H_5O_2$ peroxy radical being a common oxidation product that results in a cascade of photochemical reactions, as described in Figure 7. The resulting photochemical lifetime of C_2H_6 is typically between 1 and 3.5 years below altitudes of 5 km and much shorter (50–450 sols) above the hygropause. (Appendix A).

464

465

466

467

468

469

470

471

472

473

474

475

476

Figure 9 shows the vertical profiles of organic compounds produced by the oxidation of 50 pptv of C_2H_6 after one sol at L_S 71° and 251° , latitude 2.5° sampled at 18:00 LT, to allow comparisons against the methane investigation of Figure 3. The introduction of longer chain peroxy-radicals via the $C_2H_5O_2$ radical increases the richness of photochemical products that are produced from CH_4 oxidation. In particular, the oxidation of C_2H_6 results in CH_3CHO column averaged mixing ratios of 7.24×10^{-16} molecule/molecule at aphelion conditions, elevating to 3.18×10^{-15} molecule/molecule at perihelion conditions. UV photolysis of CH_3CHO is a source of CH_4 and carbon monoxide. We find that UV photolysis of 50 pptv homogeneous column of C_2H_6 produces a CH_4 column averaged mixing ratio of 1.87×10^{-17} molecule/molecule at aphelion, and 3.97×10^{-16} molecule/molecule at perihelion. The ratios of CH_4/C_2H_6 at aphelion and perihelion are 3.71×10^{-7} and 7.86×10^{-6} , respectively, and the ratio of CH_4/CH_3CHO at these two orbital points are 2.58×10^{-2} and 1.25×10^{-1} , respectively.

477

478

479

480

481

482

483

484

485

486

487

Formaldehyde is produced with a much higher yield for C_2H_6 oxidation than for CH_4 oxidation, resulting in a column averaged mixing ratio of 3.16×10^{-15} and 5.74×10^{-14} molecule/molecule at aphelion and perihelion, respectively. These yields are $\simeq 6$ times and 777 times higher than those made by CH_4 at aphelion and at perihelion, respectively. These higher yields of HCHO from C_2H_6 oxidation is due to a larger number of production pathways compared to the CH_4 oxidation mechanism. Production of HCOOH from C_2H_6 photochemistry during perihelion, column mixing ratio 7.30×10^{-17} molecule/molecule, is comparable with values from CH_4 oxidation, but is much smaller than CH_4 oxidation during aphelion with a column mixing ratio of 1.34×10^{-18} molecule/molecule. Lower production of HCOOH from C_2H_6 oxidation during aphelion is due to lower production pathways for $HOCH_2OOH$ and $HOCH_2O_2$, which drive subsequent production of HCOOH.

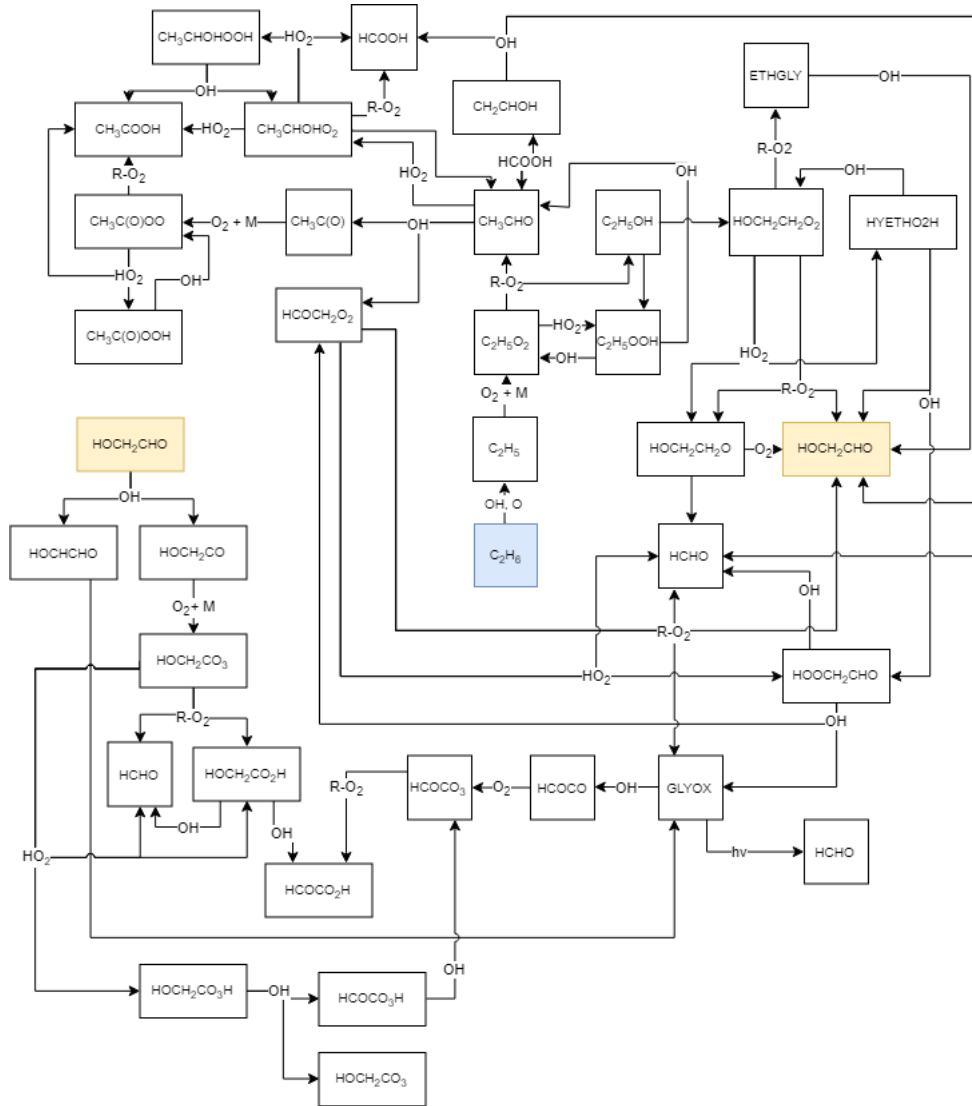


Figure 7. Primary stages of the C_2H_6 photochemistry that we use in our 1-D photochemistry submodule, taken from the CAABA/MECCA v4.0 box model.

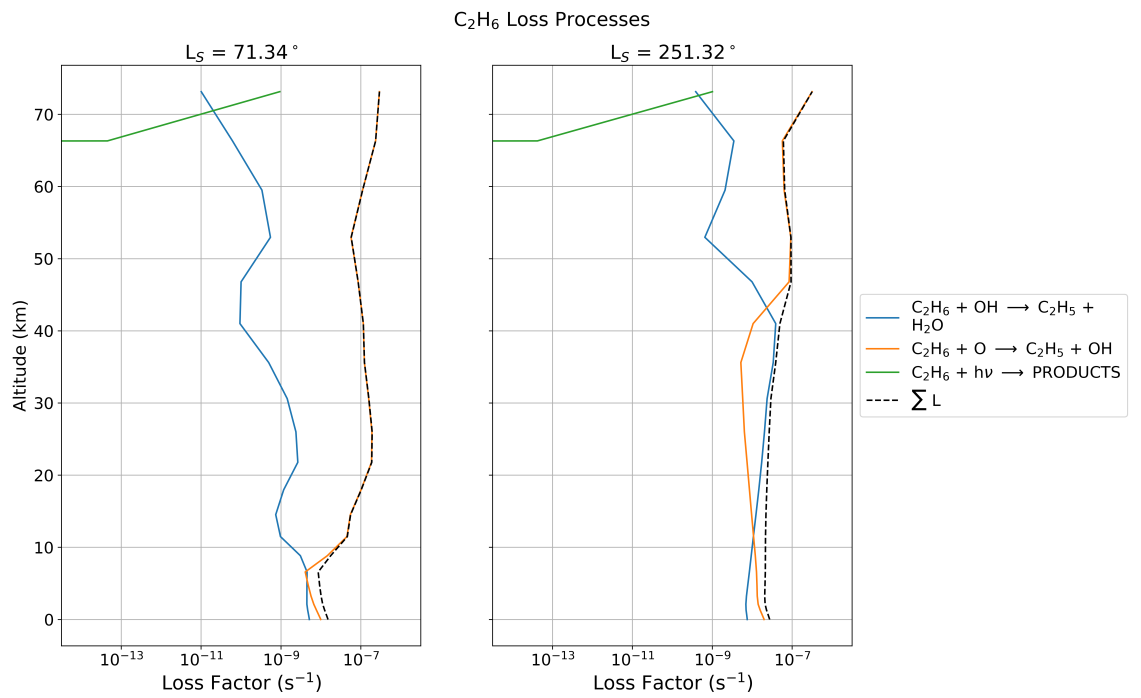


Figure 8. Photochemical loss factors for C₂H₆ as a function of altitude in our 1-D photochemistry model with altitude. Calculations are for $L_S = 71^\circ$ and 251° , 12:00 LT, at latitude $2.5^\circ N$.

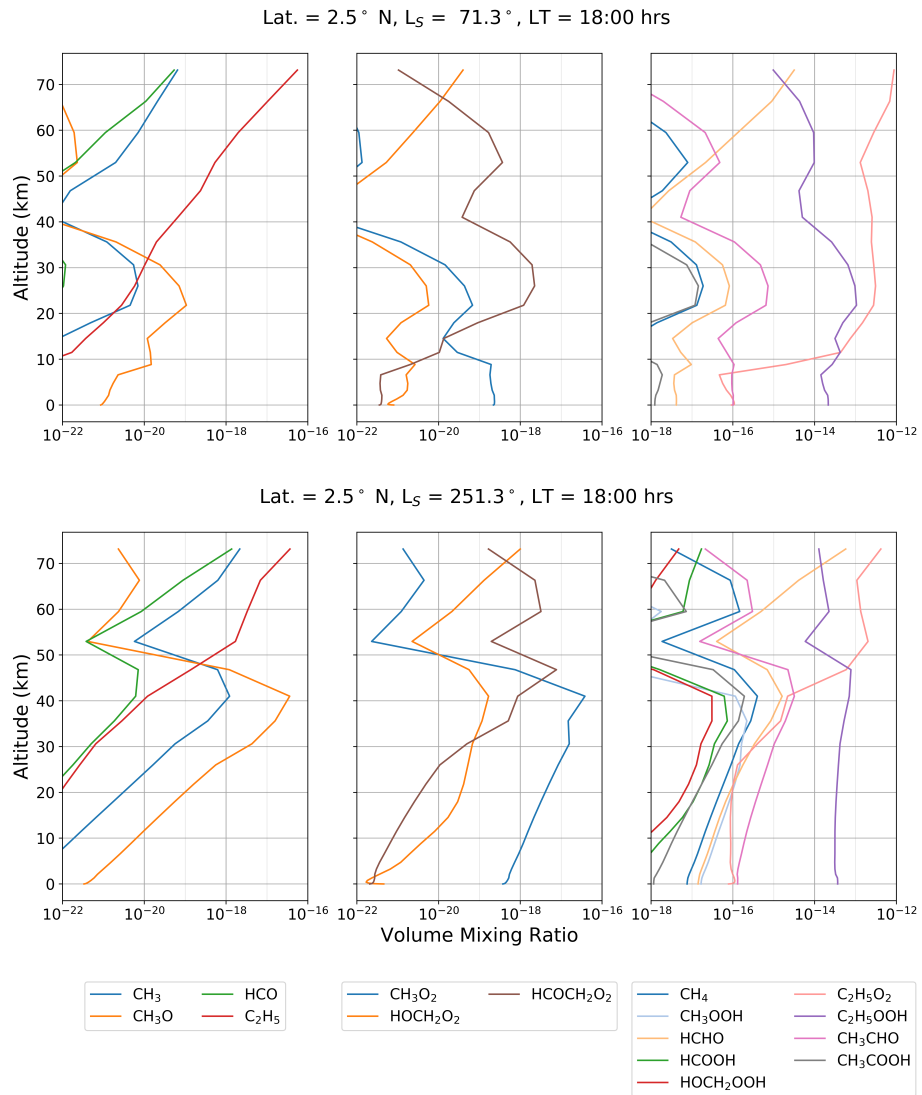


Figure 9. Volume mixing ratio profiles of oxidised organic products after one sol of introducing a uniform profile volume mixing ratio of 50 pptv of C₂H₆.

3.5 Production of Formaldehyde and Formic Acid from C₂H₆ Oxidation

Figure 10 shows the production and loss rates for HCHO and HCOOH from the oxidation of 50 pptv of C₂H₆. The largest production rate of HCHO is below the hygropause from the reaction of CH₃O₂ peroxy radical with HO₂, comparable to values from CH₄ oxidation. However, above the hygropause at 20 km the three-body reaction CH₃C(O)+O₂+M and the CH₃ radical reaction with atomic oxygen are the primary sources of HCHO. Combined, the HCHO production rate is an order of magnitude larger than the rate from CH₄ oxidation.

The higher reactivity of C₂H₆ produces a larger quantity of HOCH₂O₂ peroxy radicals and hydroperoxy radicals in the regions just above the hygropause compared to CH₄ oxidation. With no additional loss processes, the increased net production rate results in larger concentrations of HCOOH, with production falling off rapidly towards the surface.

3.6 Methane Production from the Oxidation of Acetaldehyde

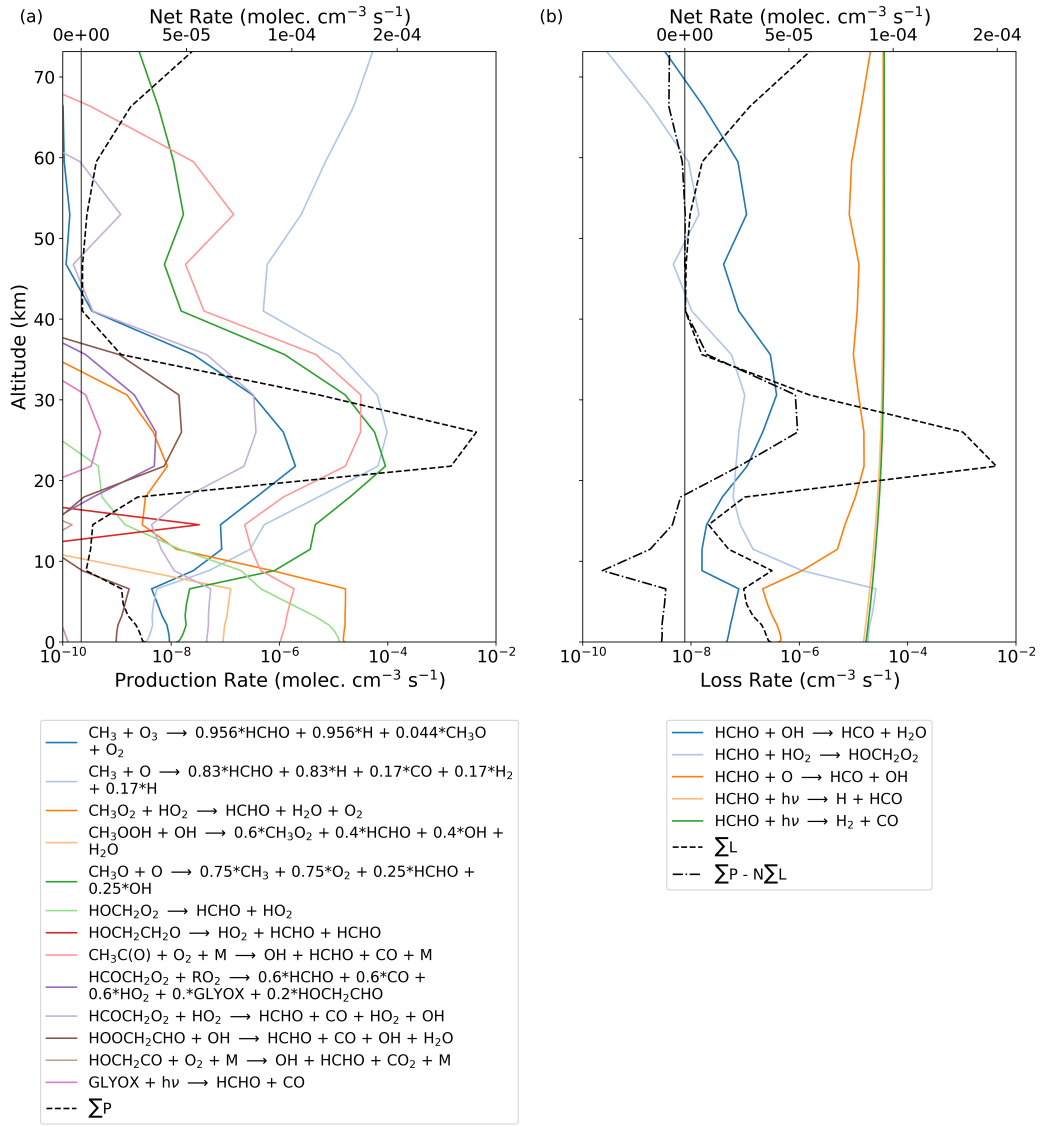
Figure 11 shows production and loss rates of CH₄ associated with a 50 pptv homogeneous column of CH₃CHO at L_S = 251°, latitude 2.5°, and at local noon to study the importance of UV photolysis of CH₃CHO. We calculate the photolysis loss rate using the TUV model (section 2) that penetrate efficiently to the surface. Net CH₄ production rates peak at 31.13 molec cm⁻³ s⁻¹, corresponding to an increase in CH₄ mixing ratio of 1.69×10⁻¹⁶ molecule/molecule s⁻¹, at ≈1.30 km above the Martian surface at this time of day. To our knowledge, this photolytic source of atmospheric CH₄ is the only proposed source that may be possible within the CO₂-dominated atmosphere of Mars.

4 Discussion and Concluding Remarks

We find that the oxidation of atmospheric CH₄ in the Martian atmosphere, at magnitudes similar to reported observations, produce formaldehyde and formic acid as photochemical products but at volume mixing ratios too low for successful detection via remote sensing by the NOMAD and ACS spectrometers aboard the ExoMars Trace Gas Orbiter. Our photochemical lifetimes of formaldehyde are consistent with previous studies (e.g., Wong and Atreya (2004)), but we have also reported variations as a function of altitude and solar longitude. Our use of the MCD v5.3 atmospheric parameters and tracer profiles enabled us to deduce that the largest atmospheric lifetimes of HCHO at latitudes less than 30° are typically around 4 hours during the northern spring and summer above the point of H₂O vapour saturation. Our model expands upon the findings from the steady state model by revealing the layered seasonal structure of HCHO that can develop, whilst refining the modelled lifetimes and revealing the seasonal variability of the compound.

Our 1-D model refines the vertical structure and seasonal variability of the CH₄ within the equatorial regions of Mars, revealing that altitudes with low water vapour content can provide O(¹D) abundances large enough to suppress the lifetime of CH₄ to between 50–100 years, shorter than previous estimates (Wong & Atreya, 2004; Summers et al., 2002; Krasnopolsky et al., 2004). We reveal a region in the upper section of the 1-D model, corresponding to 50–70 km where the absence of OH, O(¹D), and lower UV photolysis increases CH₄ lifetimes to 400–800 years during the northern spring, and to 800–1300 years during the mid-northern summer to northern winter, significantly higher than previous model estimations. Lifetimes close to the surface and below the hygropause (0–30 km) are invariant with latitude during the northern spring, but display variations between the north and southern hemisphere throughout the rest of the year, controlled by the sublimation of the respective hemispheres polar caps water ice content.

HCHO



HCOOH

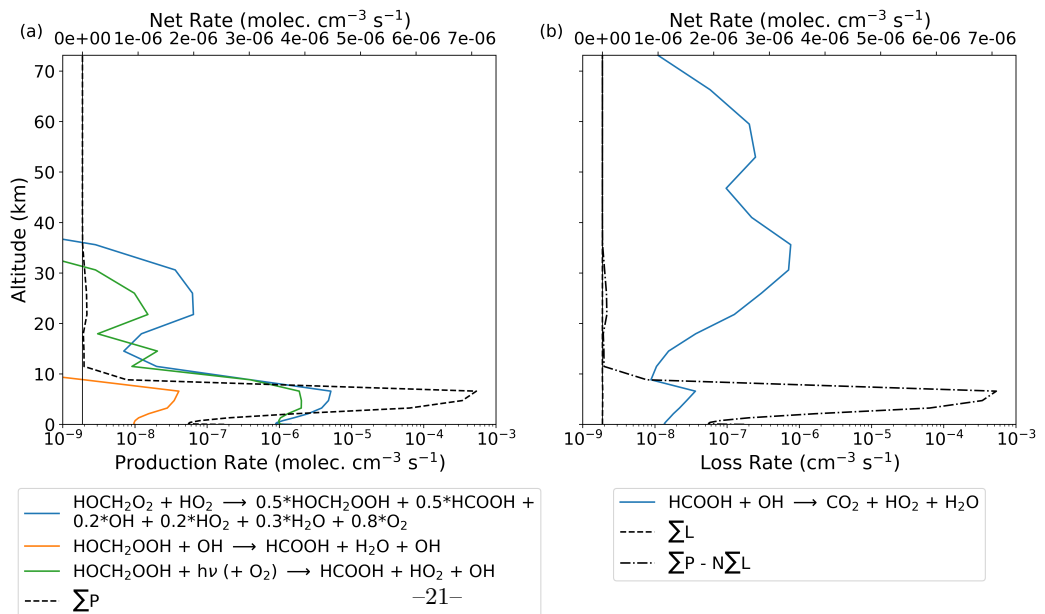


Figure 10. Photochemical production and loss rates (molec cm⁻³s⁻¹) of HCHO and HCOOH

CH₄

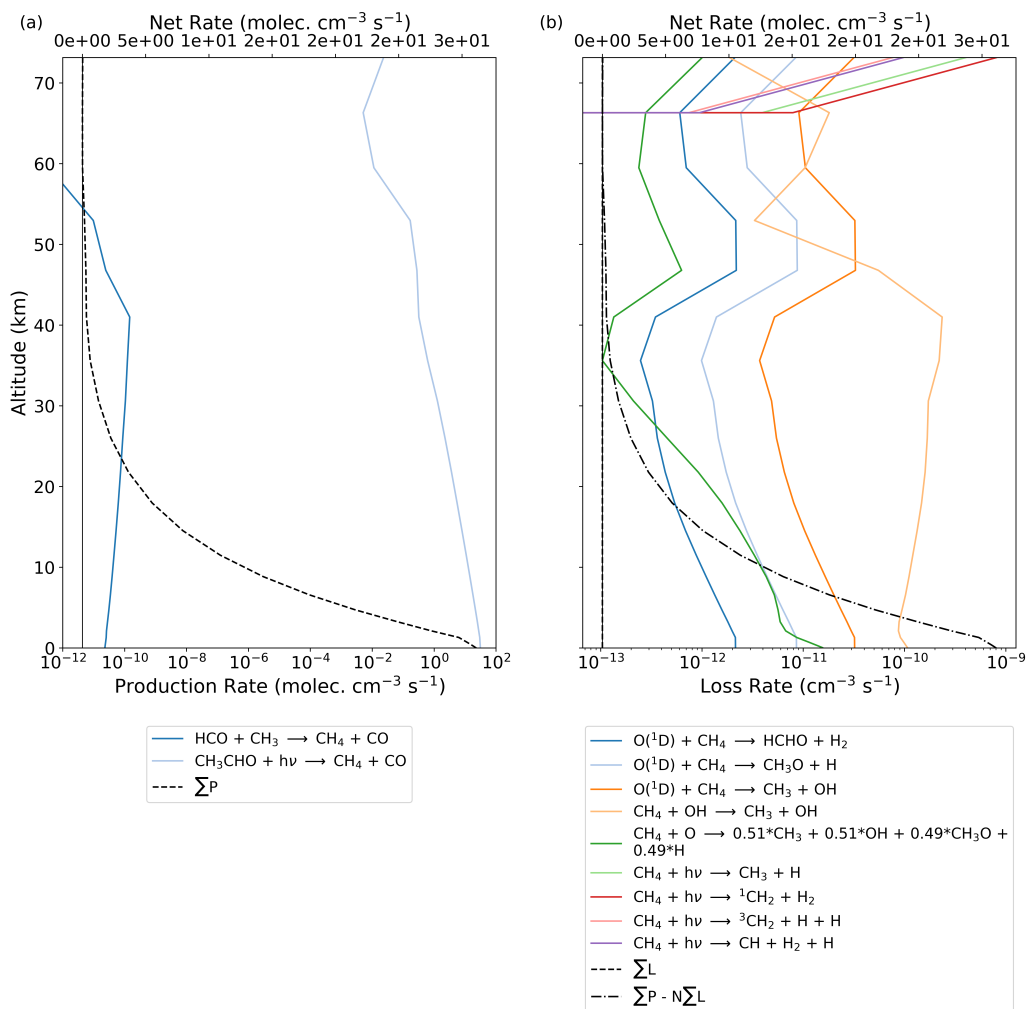


Figure 11. Photochemical production and loss rates for methane (molec cm⁻³s⁻¹), associated with the UV photolysis of a 50 pptv column of CH₃CHO, as a function of altitude. Calculations are for L_S = 251°, 12:00 LT, and latitude 2.5°N.

537 We find that the photochemical lifetime of C_2H_6 is correlated to the atmospheric
 538 water vapour content on Mars. Within the hygropause, lifetimes are found to be within
 539 3–4 years, where OH is the dominant photochemical sink. At higher altitudes, these life-
 540 times are reduced to 100–400 Mars sols (0.15–0.6 years), due to the higher abundance
 541 of atomic oxygen. The lifetimes of acetaldehyde reach values of approximately one sol
 542 close to the Martian surface across all equatorial latitudes during the northern spring,
 543 that lower to roughly 0.5 sols in the northern hemisphere summer to winter periods. Acetic
 544 acid displays a similar seasonal trend, with lifetimes in the northern spring being between
 545 3 and 4 sols below the hygropause, and lowering to between 0.2–1 sol with the eleva-
 546 tion of the water saturation point. Oxidation of C_2H_6 in the Martian atmosphere results
 547 in a distinct profile of acetaldehyde, as well as greater yields of HCHO and HCOOH, com-
 548 pared to CH_4 oxidation. The 1-D model predicts atmospheric lifetimes of between 15
 549 and 32 hours below altitudes of 25 km during $L_S = 0-135^\circ$, lowering to 4–12 hours out-
 550 side of this time frame across all equatorial latitudes, for CH_3CHO . We therefore pro-
 551 pose that any instrument detection of CH_3CHO can be attributed to a surface release
 552 of C_2H_6 within the immediate local environment of the site of observation.

553 Our more comprehensive description of atmospheric chemistry, involving 135 or-
 554 ganic reactions, significantly expands on the schemes used by Wong and Atreya (2004)
 555 and Summers et al. (2002). No formic acid was reported by the model of Wong and Atreya
 556 (2004) for their 1-D steady state model with 100 ppmv of CH_4 , whereas we report vol-
 557 ume mixing ratios of similar magnitude to HCHO below the hygropause with CH_4 abun-
 558 dances of 50 pptv, the current upper limit on Mars derived in Korablev et al. (2019). This
 559 discrepancy can be explained by our more detailed description of peroxy radical chem-
 560 istry that is taken from the CAABA/MECCA v4.0 chemistry scheme. In our 1-D model,
 561 photochemical lifetimes of HCOOH are inversely proportional to the abundance of OH
 562 available. At the top of the hygropause, lifetimes have magnitudes of 1 - 10 sols. Below,
 563 the lifetimes vary substantially depending on the water vapour availability. Below 5 km,
 564 photochemical lifetimes in the drier southern latitudes can reach values exceeding 10^3
 565 sols, whereas in the north, values between 10 and 100 are commonly found. These long
 566 photochemical lifetimes of HCOOH, in comparison to HCHO, makes it the most likely
 567 photochemical product of CH_4 oxidation that could provide independent verification of
 568 CH_4 . Spectral features of HCOOH lie within the IR wavelengths measured by the ACS
 569 aboard the TGO, and the long wave channel of the PFS covers the wavenumber range
 570 of 250–1700 cm^{-1} (Formisano et al., 2005) that includes two absorption features of the
 571 HCOOH molecule (Gordon et al., 2017).

572 We find that the introduction of CH_4 at magnitudes similar to an empirically de-
 573 rived upper limit (<50 pptv) fails to produce significant perturbations to CO, O_3 , or H_2O
 574 vapour (not shown) that will be observable by instruments aboard the TGO. CH_4 reactions
 575 with $O(^1D)$ above the hygropause and below 50 km have the net effect of increasing OH
 576 concentrations by magnitudes of $10^{-3}\%$ after one sol of exposure, which results in cat-
 577 alyzing the conversion of CO to CO_2 via reaction e₁ of B1. The increase in OH arises
 578 from the previously described reactions of $O(^1D)$ atoms reacting with CH_4 in the drier
 579 altitudes, most notably reaction b₇. CO experiences relative perturbations of $-10^{-6}\%$
 580 in the mid-altitudes, which will be lost within instrumental noise. This rise in OH, and
 581 the loss of $O(^1D)$ to CH_4 interactions and $O(^3P)$ with organic radical interactions, re-
 582 sults in a drop in O_3 production in this region and increased O_3 loss. These perturba-
 583 tions are small, however, with drops of $10^{-3}\%$ after one sol, an amount that is below in-
 584 strument signal-to-noise values. This highlights that source regions of CH_4 will not be
 585 identifiable by perturbations made to inorganic trace gas species observable to the Ex-
 586 oMars Trace Gas Orbiter.

587 Finally, our model highlights the possible existence of an atmospheric source of CH_4
 588 from the photolysis of CH_3CHO , an oxidation product of C_2H_6 . Photolysis of CH_3CHO
 589 in the Martian atmosphere is capable of producing trace amounts of CH_4 at all altitudes

590 above the surface. We find that 50 pptv of CH_3CHO is capable of producing CH_4 at a
 591 volume mixing ratio rate of $4.54 \times 10^{-16} \text{ s}^{-1}$.

592 This opens up the possibility of further studying CH_3CHO as a possible source for
 593 CH_4 detection on Mars. Although no evidence exists for CH_3CHO on Mars, one hypo-
 594 theoretical source could be due to a sub-surface acetylene hydratase (Rosner & Schink, 1995)
 595 enzyme that converts acetylene (C_2H_2) to CH_3CHO through reactions with liquid wa-
 596 ter.

597 **Appendix A Martian Atmospheric Lifetimes of Methane, Formalde-** 598 **hyde, Formic Acid, and Ethane**

599 **A1 Methane**

600 Figure A1 shows the net atmospheric lifetime of CH_4 , incorporating all loss terms
 601 (Figure 2), as a function of latitude and solar longitude. Atmospheric lifetimes reach a
 602 minimum of 25–400 year between the top of the hygropause and approximately 50 km
 603 due to the larger abundance of the $\text{O}(^1\text{D})$ atom. Below the hygropause where OH is the
 604 dominant sink, atmospheric lifetimes vary between 400 and 800 years. The longest life-
 605 times of 800–1600 years lie between 50 and 60 km during winter ($L_S = 270\text{--}360^\circ$), as de-
 606 scribed above, where the OH and $\text{O}(^1\text{D})$ loss processes decline and before photolysis dom-
 607 inates above 60 km.

608 Variations in atmospheric lifetime are driven by the position of the Martian hygropause
 609 and the water vapour content beneath, which is determined by 3-D model output from
 610 the MCD (section 2). Water vapour columns reach their maximum during hemispheric
 611 summer months when polar water ice sublimates with rising atmospheric temperatures.
 612 SPICAM water vapour column measurements at $L_S = 50^\circ$ (Fedorova et al., 2006) show
 613 only small variations at latitudes less than 30° , with values ranging from 2–10 pr μm ,
 614 with saturation values under 25 km. This is consistent with our model loss processes that
 615 determine the variation in atmospheric lifetime. Above 50 km, the stronger flux of so-
 616 lar radiation in the northern hemisphere due to the planets axial tilt results in a larger
 617 abundance of $\text{O}(^1\text{D})$ and a subsequent lower photochemical lifetime of CH_4 than in the
 618 southern hemisphere. As water vapour column abundances and saturation altitudes in-
 619 crease with L_S , the low latitude atmospheric lifetime of CH_4 increases below 50 km due
 620 to H_2O reacting with $\text{O}(^1\text{D})$ and decreases below roughly 25 km. The decrease in solar
 621 flux during northern autumn and winter months ($L_S = 180^\circ\text{--}360^\circ$) reduces the produc-
 622 tion rate of $\text{O}(^1\text{D})$ relative to the southern hemisphere, which explains the variation in
 623 lifetimes between the hemispheres.

624 **A2 Formaldehyde**

625 Figure A2 shows the resultant seasonal variability of HCHO lifetime at latitudes
 626 30°N , 2.5°N , and 30°S . We find the longest lifetimes, between 4 and 5 hours, are found
 627 below 5 km in the southern hemisphere during the northern summer/southern winter,
 628 when this region contains low levels of water vapour.

629 **A3 Formic Acid**

630 Figure A3 shows the resultant seasonal variability of HCOOH lifetime at latitudes
 631 30°N , 2.5°N , and 30°S . The lifetime of HCOOH is anti-correlated with water vapour,
 632 as expected. The longest lifetime (of magnitude's greater than 10^4 sols) is during the north-
 633 ern spring at altitudes greater than 60 km where OH is lowest. As OH values increase
 634 with the supply of water vapour from northern polar ice sublimation, atmospheric life-
 635 times falls to 1–10 sols close to the hygropause and 10–200 sols at lower altitudes closer
 636 to the surface (below 5 km).

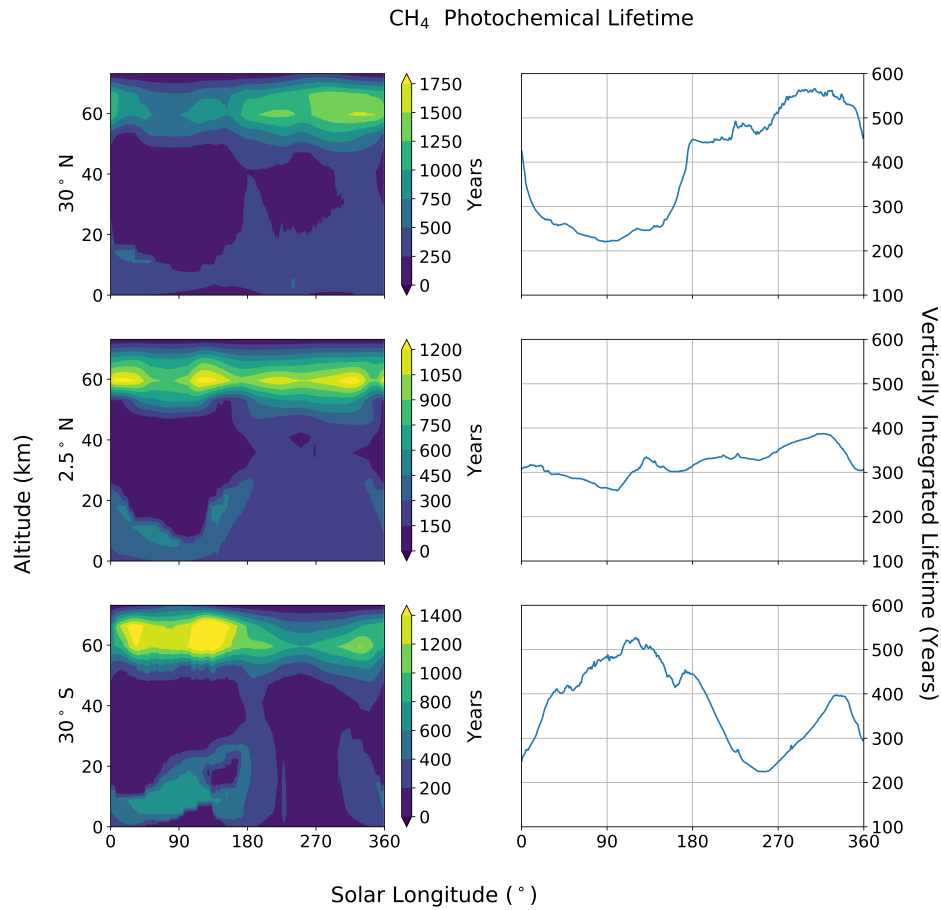


Figure A1. Local and vertically integrated photochemical lifetime of CH₄ within the atmosphere of Mars and its variations with altitude (km) and solar longitude at latitudes 30°N, 2.5°N, and 30°S, respectively. All vertical segments are values from the 1-D photochemistry model at 12:00 LT.

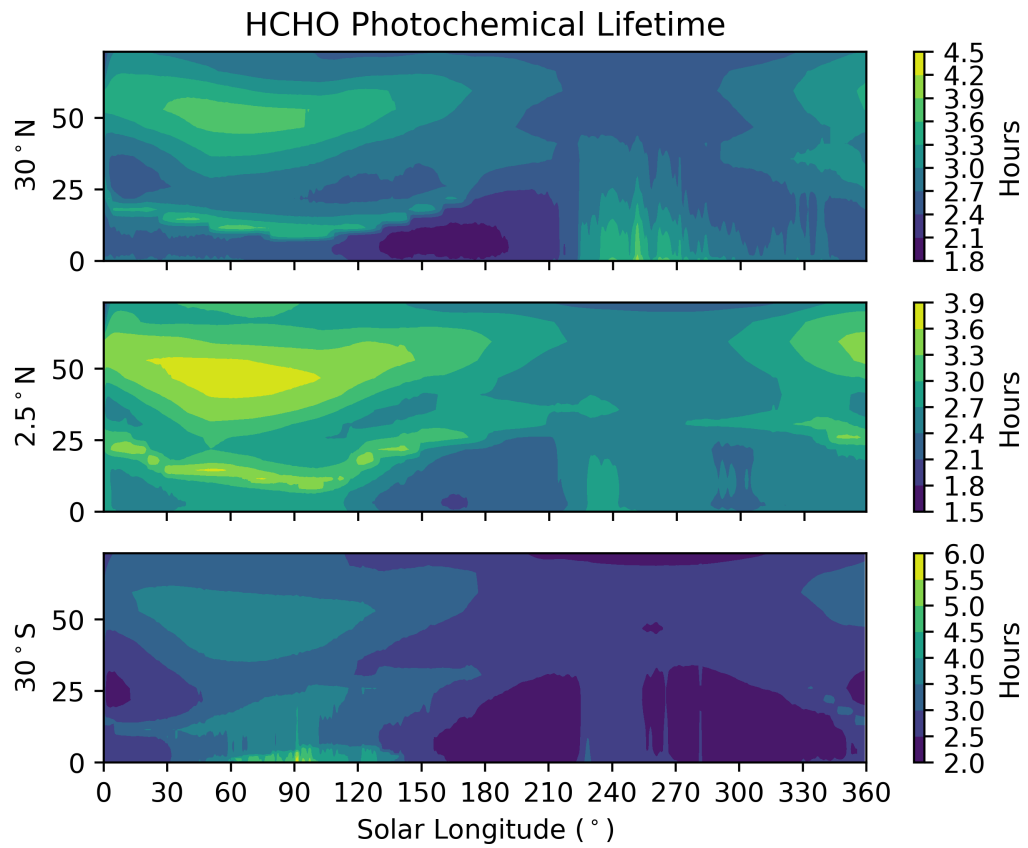


Figure A2. Photochemical lifetime of HCHO within the atmosphere of Mars and its variations with altitude (km) and solar longitude at latitudes 30°N, 2.5 °N, and 30°S, respectively. All vertical segments are values from the 1-D photochemistry model at 12:00 LT.

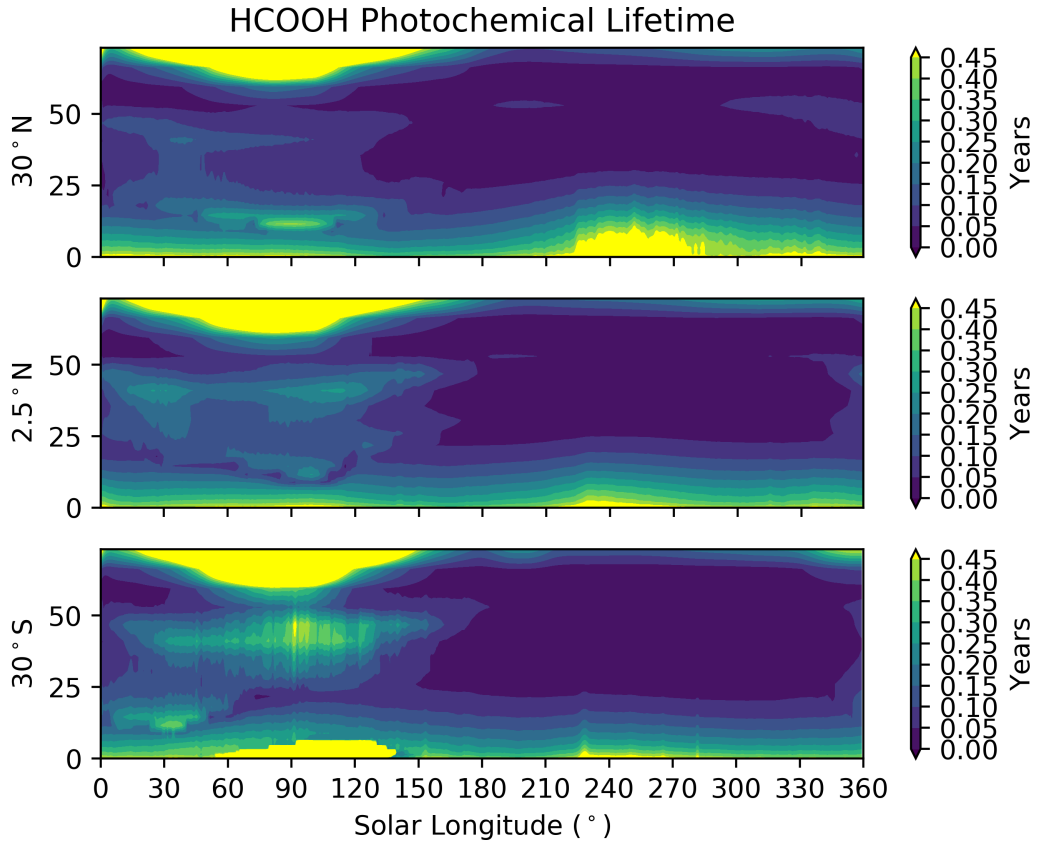


Figure A3. Photochemical lifetime of HCOOH within the atmosphere of Mars and its variations with altitude (km) and solar longitude at latitudes 30°N, 2.5 °N, and 30°S, respectively. All vertical segments are values from the 1-D photochemistry model at 12:00 LT. Contour map saturated for values greater than 0.45 years.

637 With atmospheric lifetimes of this length, describing seasonal changes in HCOOH
 638 profiles using a 1-D photochemistry model becomes problematic due to the photochem-
 639 ical lifetimes exceeding the venting timescales associated with our 3.75° thick zonal band
 640 that our model represents. Without horizontal transport equations to describe the loss
 641 of HCOOH to the zonal band edges, the resultant profiles after a one-year 1-D model
 642 run will be subject to gross inaccuracies. As previously discussed in section 2, solving
 643 the 1-D model equation for steady state conditions will not yield useful information due
 644 to the observed temporal and localized nature of CH₄ emissions, invalidating the notion
 645 of a steady-state environment.

646 **A4 Ethane**

647 Figure A4 shows that C₂H₆ has longer photochemical lifetimes below the points
 648 of H₂O saturation, where we find typical values that range from 3 to 5 years. In the mid-
 649 dle atmosphere, the large abundance of O(³P) reduced the lifetime to 30–450 sols. Based
 650 on these calculations, we suggest that any detection of C₂H₆ made by the TGO instru-
 651 ments will due to an active release.

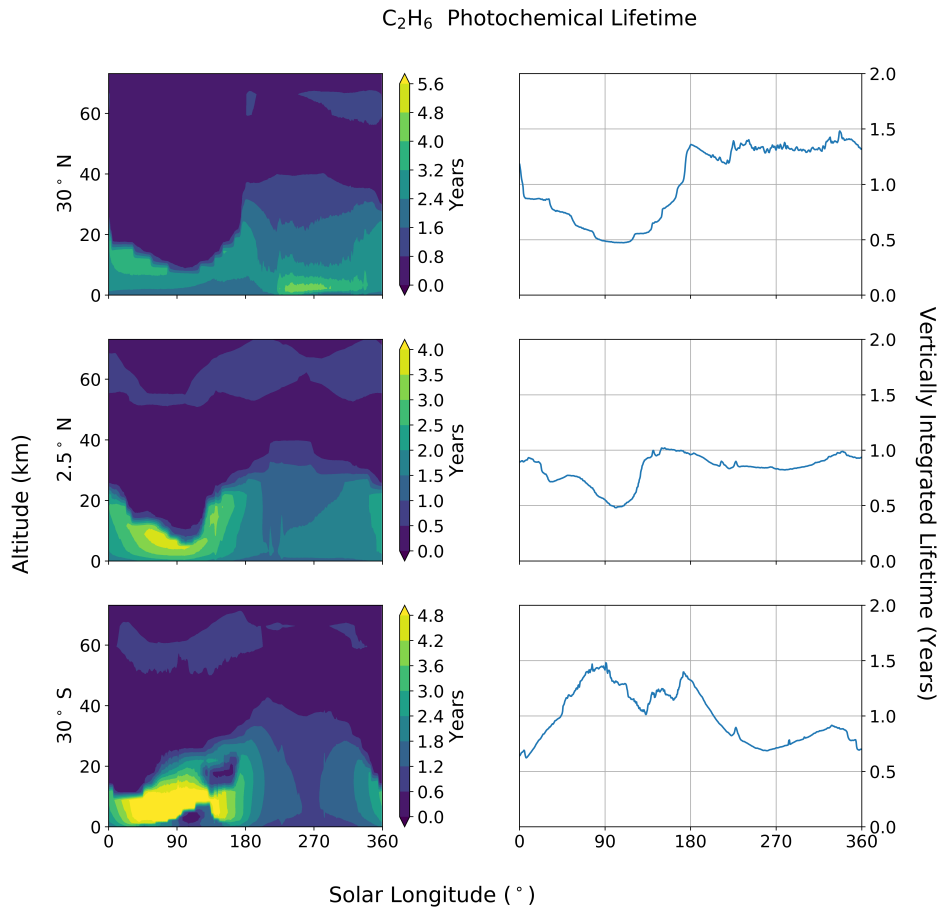


Figure A4. Local and vertically integrated photochemical lifetime of C_2H_6 within the atmosphere of Mars and its variations with altitude (km) and solar longitude at latitudes 30°N, 2.5°N, and 30°S, respectively. All vertical segments are values from the 1-D photochemistry model at 12:00 LT.

Table B1. Inorganic reaction rate coefficients within the 1-D photochemistry submodule. Bimolecular rate coefficient units are $\text{cm}^3 \text{molec}^{-1} \text{s}^{-1}$. Values denoted by superscript *a* are three-body reactions with values taken with atmospheric number density complying to temperatures of $T = 298 \text{ K}$ and pressures of 660 Pa .

Key	Reaction	Formula	Rate at T = 298 K	Reference
Reactions with O				
<i>a</i> ₁	$O + O_2 + M \rightarrow O_3 + M$	$2.075 \times 6.00E-34(T/300)^{-2.4}$	$2.23E-16^a$	(S. Sander et al., 2003)
<i>a</i> ₂	$O + O + M \rightarrow O_2 + M$	$2.50 \times 9.46E-34 \exp(485/T)$	$2.10E-15^a$	(Campbell & Gray, 1973)
<i>a</i> ₃	$O + O_3 \rightarrow O_2 + O_2$	$8.00E-13 \exp(-2060/T)$	$7.96E-16$	(S. Sander et al., 2003)
Reactions with O(¹ D)				
<i>b</i> ₁	$O(^1D) + CO_2 \rightarrow O + CO_2$	$7.40E-11 \exp(120/T)$	$1.11E-10$	(S. Sander et al., 2003)
<i>b</i> ₂	$O(^1D) + H_2O \rightarrow OH + OH$	$1.63E-10 \exp(60/T)$	$1.99E-10$	(S. Sander et al., 2006)
<i>b</i> ₃	$O(^1D) + H_2 \rightarrow OH + H$	$1.20E-10$	$1.20E-10$	(S. Sander et al., 2011)
<i>b</i> ₄	$O(^1D) + O_2 \rightarrow O + O_2$	$3.30E-11 \exp(55/T)$	$3.97E-11$	(S. Sander et al., 2006)
<i>b</i> ₅	$O(^1D) + O_3 \rightarrow O_2 + O_2$	$1.20E-11$	$1.20E-11$	(S. Sander et al., 2003)
<i>b</i> ₆	$O(^1D) + O_3 \rightarrow O_2 + O + O$	$1.20E-11$	$1.20E-11$	(S. Sander et al., 2003)
<i>b</i> ₇	$O(^1D) + CH_4 \rightarrow CH_3 + OH$	$0.75 \times 1.75E-10$	$1.31E-10$	(S. Sander et al., 2003)
<i>b</i> ₈	$O(^1D) + CH_4 \rightarrow CH_3O + H$	$0.20 \times 1.75E-10$	$3.50E-11$	(S. Sander et al., 2003)
<i>b</i> ₉	$O(^1D) + CH_4 \rightarrow HCHO + H_2$	$0.05 \times 1.75E-10$	$8.75E-12$	(S. Sander et al., 2003)
Reactions with Hydrogen Compounds				
<i>c</i> ₁	$O + HO_2 \rightarrow OH + O_2$	$3.00E-11 \exp(200/T)$	$5.87E-11$	(S. Sander et al., 2003)
<i>c</i> ₂	$O + OH \rightarrow O_2 + H$	$1.80E-11 \exp(180/T)$	$3.29E-11$	(S. Sander et al., 2011)
<i>c</i> ₃	$H + O_3 \rightarrow OH + O_2$	$1.40E-10 \exp(-470/T)$	$2.89E-11$	(S. Sander et al., 2003)
<i>c</i> ₄	$H + HO_2 \rightarrow OH + OH$	$7.20E-11$	$7.20E-11$	(S. Sander et al., 2006)
<i>c</i> ₅	$H + HO_2 \rightarrow H_2 + O_2$	$6.90E-12$	$6.90E-12$	(S. Sander et al., 2006)
<i>c</i> ₆	$H + HO_2 \rightarrow H_2O + O$	$1.60E-12$	$1.60E-12$	(S. Sander et al., 2006)
<i>c</i> ₇	$OH + HO_2 \rightarrow H_2O + O_2$	$4.80E-11 \exp(250/T)$	$1.11E-10$	(S. Sander et al., 2003)
<i>c</i> ₈	$HO_2 + HO_2 \rightarrow H_2O_2 + O_2$	$1.50E-12 \exp(19/T)$	$1.60E-12$	(Christensen et al., 2002)
<i>c</i> ₉	$OH + H_2O_2 \rightarrow H_2O + HO_2$	$1.80E-12$	$1.80E-12$	(S. Sander et al., 2006)
<i>c</i> ₁₀	$OH + H_2 \rightarrow H_2O + H$	$2.80E-12 \exp(-1800/T)$	$6.67E-15$	(S. Sander et al., 2006)
<i>c</i> ₁₁	$H + O_2 + M \rightarrow HO_2 + M$	$k_{\text{3rd}}(2.5 \times 4.4E-32, -1.3, 7.5E-11, 0.2)$	$1.88E-14^a$	(S. Sander et al., 2011)
<i>c</i> ₁₂	$O + H_2O_2 \rightarrow OH + HO_2$	$1.40E-12 \exp(-2000/T)$	$1.70E-15$	(S. Sander et al., 2003)
<i>c</i> ₁₃	$OH + OH \rightarrow H_2O + O$	$1.80E-12$	$1.80E-12$	(S. Sander et al., 2006)
<i>c</i> ₁₄	$OH + O_3 \rightarrow HO_2 + O_2$	$1.50E-12 \exp(-880/T)$	$7.83E-14$	(S. Sander et al., 2003)
<i>c</i> ₁₅	$HO_2 + O_3 \rightarrow OH + O_2 + O_2$	$1.00E-14 \exp(-490/T)$	$1.93E-15$	(S. Sander et al., 2003)
<i>c</i> ₁₆	$HO_2 + HO_2 + M \rightarrow H_2O_2 + O_2 + M$	$2.50 \times 2.10E-33 \exp(920/T)$	$2.01E-14^a$	(S. Sander et al., 2011)
<i>c</i> ₁₇	$OH + OH + M \rightarrow H_2O_2 + M$	$k_{\text{3rd}}(2.5 \times 6.9E-31, -1, 2.60E-11, 0)$	$2.70E-13^a$	(S. Sander et al., 2003)
<i>c</i> ₁₈	$H + H + M \rightarrow H_2 + M$	$2.5 \times 1.80E-30/T$	$2.64E-14^a$	(Baulch et al., 2005)
Carbon Compounds				
<i>e</i> ₁	$OH + CO \rightarrow CO_2 + H$	Details in Joshi and Wang (2006)	$1.47E-13$	(Joshi & Wang, 2006)
<i>e</i> ₂	$O + CO + M \rightarrow CO_2 + M$	$2.5 \times 6.50E-33 \exp(-2184/T)$	$1.87E-18^a$	(Tsang & Hampson, 1986)

Appendix B Reaction Rate Coefficients

Table B2. Photolytic reactions of inorganic compounds used within the 1-D photochemistry submodule. Values (s^{-1}) are interpolated from an offline look-up table constructed by a modified TUV (Madronich et al., 2002) model with respect to CO_2 and O_3 column abundances overhead, temperature, optical opacity and solar zenith angle. Values displayed are for a solar zenith angle of 0° , $L_S = 251^\circ$ (perihelion).

Key	Reaction	$J(z = 0.50 \text{ km})$	$J(z = 42.67 \text{ km})$
$j_{\text{O}_2 \rightarrow \text{O}}$	$\text{O}_2 + h\nu \rightarrow \text{O} + \text{O}$	2.95E-10	5.16E-09
$j_{\text{O}_2 \rightarrow \text{O}(^1D)}$	$\text{O}_2 + h\nu \rightarrow \text{O} + \text{O}(^1D)$	0	0
$j_{\text{CO}_2 \rightarrow \text{O}}$	$\text{CO}_2 + h\nu \rightarrow \text{CO} + \text{O}$	3.79E-12	1.02E-10
$j_{\text{CO}_2 \rightarrow \text{O}(^1D)}$	$\text{CO}_2 + h\nu \rightarrow \text{CO} + \text{O}(^1D)$	0	0
$j_{\text{O}_3 \rightarrow \text{O}(^1D)}$	$\text{O}_3 + h\nu \rightarrow \text{O}_2 + \text{O}(^1D)$	3.12E-03	4.09E-03
$j_{\text{O}_3 \rightarrow \text{O}}$	$\text{O}_3 + h\nu \rightarrow \text{O}_2 + \text{O}$	5.22E-04	6.86E-04
$j_{\text{H}_2\text{O}}$	$\text{H}_2\text{O} + h\nu \rightarrow \text{H} + \text{OH}$	1.28E-10	4.67E-08
$j_{\text{H}_2\text{O}_2}$	$\text{H}_2\text{O}_2 + h\nu \rightarrow \text{OH} + \text{OH}$	3.93E-05	5.26E-05
j_{HO_2}	$\text{HO}_2 + h\nu \rightarrow \text{O} + \text{OH}$	2.40E-04	3.20E-04

Acknowledgments

We gratefully acknowledge Stephen Lewis for providing the 1-D atmospheric chemistry sub-module of the LMD-UK MGCM. We also thank Manish Patel for providing insights into Trace Gas Orbiter instruments, and thank Rolf Sander for maintaining the CAABA/MECCA Box model, published under the GNU GPL, which we have used to develop our description of Mars' photochemistry. We thank Sasha Madronich and the National Center for Atmospheric Research for providing the source code of the Tropospheric and Ultraviolet Radiation model used to construct the offline look-up table of photolysis rates of organic compounds that the 1-D model interpolates from. B.M.T. acknowledges his PhD studentship funding (ST/1/R001324/1) from the UK Space Agency, administered by the Science and Technology Facilities Council, as part of the Aurora science programme.

The 1-D photochemistry model code used to construct this work has been frozen and stored on Zenodo, (Taysum, 2020a).

The datasets containing the atmospheric parameters and tracer mixing ratio profiles constructed from the Mars Climate Database v5.3 are also stored on Zenodo, (Taysum, 2020b).

All output files produced by the 1-D model used in this work, and plotting routines used to construct the figures and extract numerical data from the files, are stored on Zenodo, (Taysum, 2020c).

The TUV model source code used to construct the J-value look-up tables can be acquired through the url <https://www2.acom.ucar.edu/modeling/tropospheric-ultraviolet-and-visible-tuv-radiation-model>.

The Mars Climate Database v5.3 source code used to create the offline tables for atmospheric parameter and long-lived tracer vmr's for the 1-D model here can be acquired through the url <http://www-mars.lmd.jussieu.fr/mars/access.html>, requiring a request to be made to the researchers listed on the site.

References

Atkinson, R., Baulch, D. L., Cox, R. A., Crowley, J. N., Hampson, R. F., Hynes,

Table B3. Functions and constants used by the R-O₂ permutation reaction handling scheme extracted from the CAABA/MECCA v4.0 box model.

CAABA/MECCA v4.0 Reaction Rate Parameters		
Key	Formula	Notes and Citations
Radical Arrhenius Equations		
k_ch3o2	1.03E-13*exp(365/T)	CH ₃ O ₂ Self-reaction (R. Sander et al., 2019)
k_ch3ooh	5.30E-12*exp(190/T)	CH ₃ OOH + OH Reaction (R. Sander et al., 2019)
k_ch3co2h	4.00E-14*exp(850/T)	CH ₃ CO ₂ H + OH Reaction (R. Sander et al., 2019)
k_ro2ho2_1	2.91E-13*exp(1300/T)*(1 - exp(-0.245*1))	RO ₂ + HO ₂ (One carbon atom) (R. Sander et al., 2019)
k_ro2ho2_2	2.91E-13*exp(1300/T)*(1 - exp(-0.245*2))	RO ₂ + HO ₂ (Two carbon atoms) (R. Sander et al., 2019)
Arrhenius Equations for H Abstraction by OH		
k_s	4.50E-18*T ² *exp(253./T)	(Taraborrelli, 2010; R. Sander et al., 2019)
k_t	2.12E-18*T ² *exp(696/T)	(Taraborrelli, 2010; R. Sander et al., 2019)
k_rohro	2.10E-18*T ² *exp(-85/T)	(Taraborrelli, 2010; R. Sander et al., 2019)
k_roohro	0.60*k_ch3ooh	(Taraborrelli, 2010; R. Sander et al., 2019)
k_co2h	0.7*k_ch3co2h	(Taraborrelli, 2010; R. Sander et al., 2019)
kdec	1.00E6	(Atkinson et al., 2006; R. Sander et al., 2019)
Updated Rate Constants for RO ₃ + HO ₂ Reactions		
kapho2	5.20E-13*exp(980/T)*1.865	(Groß et al., 2014; R. Sander et al., 2019)
Arrhenius Equations for Permutation Reactions		
k_ro2soro2	2*(7.70E-15*exp(1330/T)*k_ch3o2) ^{0.5}	(R. Sander et al., 2019)
k_ro2rco3	4.00E-12*exp(500/T)	(R. Sander et al., 2019)
k_ro2poro2	2*7.50E-14*exp(500/T)	(R. Sander et al., 2019)
Substituent Factors		
f_soh	3.44	(Taraborrelli, 2010; R. Sander et al., 2019)
f_sooh	8.00	(Taraborrelli, 2010; R. Sander et al., 2019)
f_pch2oh	1.29	(Taraborrelli, 2010; R. Sander et al., 2019)
f_tooh	8.00	(Taraborrelli, 2010; R. Sander et al., 2019)
f_toh	2.68	(Taraborrelli, 2010; R. Sander et al., 2019)
f_o	8.15	(Taraborrelli, 2010; R. Sander et al., 2019)
f_cho	0.55	(Taraborrelli, 2010; R. Sander et al., 2019)
f_co2h	1.67	(Taraborrelli, 2010; R. Sander et al., 2019)
Branching Ratios for RO ₂ + HO ₂ Reactions		
rco3_o3	0.10	(Groß et al., 2014; R. Sander et al., 2019)
rco3_oh	0.69	(Groß et al., 2014; R. Sander et al., 2019)
rco3_ooh	0.21	(Groß et al., 2014; R. Sander et al., 2019)
rchoch2o2_oh	0.10	(R. Sander et al., 2019)
rcoch2o2_oh	0.15	(R. Sander et al., 2019)
rcoch2o2_ooh	0.85	(R. Sander et al., 2019)

Table B4. Chemical reactions and rate coefficients involved in the oxidation of CH₄ used in our 1-D photochemistry model. Bimolecular rate coefficient units are cm³ molec⁻¹ s⁻¹. ^a are three-body reactions with values taken with atmospheric number density complying to temperatures of T = 298 K and pressures of 660 Pa. ^b are unimolecular rate coefficients with units s⁻¹.

Methane Reaction Scheme				
Key	Reaction	Formula	Rate at T = 298 K	Reference
<i>cab</i> ₁	CH ₄ + OH → CH ₃ + OH	1.85E-20exp(2.82LOG(T) - 987./T)	6.40E-15	(R. Sander et al., 2019)
<i>cab</i> ₂	CH ₄ + O → 0.51 * CH ₃ + 0.51 * OH +0.49 * CH ₃ O + 0.49 * H	6.03E-18(T ^{2.17})exp(-3619/T)	7.50E-18	(R. Sander et al., 2019)
<i>cab</i> ₃	CH ₃ + O ₂ + M → CH ₃ O ₂ + M	k.3rd(7.00E-31, 3., 1.80E-12, -1.1)	1.14E-13 ^a	(R. Sander et al., 2019)
<i>cab</i> ₄	CH ₃ + O ₃ → 0.956 * HCHO + 0.956 * H +0.044 * CH ₃ O + O ₂	5.10E-12exp(-210/T)	2.52E-12	(R. Sander et al., 2019)
<i>cab</i> ₅	CH ₃ + O → 0.83 * HCHO + 0.83 * H +0.17 * CO + 0.17 * H ₂ + 0.17 * H	1.30E-10	1.3E-10	(R. Sander et al., 2019)
<i>cab</i> ₆	CH ₃ O ₂ + HO ₂ → CH ₃ OOH + O ₂	3.8E-13exp(780/T) /(1 + 1/(498exp(1160/T)))	5.21E-12	(R. Sander et al., 2019)
<i>cab</i> ₇	CH ₃ O ₂ + HO ₂ → HCHO + H ₂ O + O ₂	3.8E-13exp(780/T) /(1 + 498exp(-1160/T))	4.67E-13	(R. Sander et al., 2019)
<i>cab</i> ₈	CH ₃ O ₂ + R - O ₂ → CH ₃ O + 0.5 * O ₂	2 × 7.40E-13exp(-520/T)	2.59E-13	(R. Sander et al., 2019)
<i>cab</i> ₉	CH ₃ O ₂ + R - O ₂ → 0.5 * HCHO +0.5 * CH ₃ OH + 0.5 * O ₂	2 × (k.ch3o2 - 7.40E-13exp(-520/T))	4.43E-13	(R. Sander et al., 2019)
<i>cab</i> ₁₀	CH ₃ O ₂ + O ₃ → CH ₃ O + O ₂ + O ₂	2.90E-16exp(-1000/T)	1.01E-17	(R. Sander et al., 2019)
<i>cab</i> ₁₁	CH ₃ O ₂ + OH → CH ₃ O + HO ₂	1.40E-10	1.40E-10	(R. Sander et al., 2019)
<i>cab</i> ₁₂	CH ₃ O ₂ + O → CH ₃ O + O ₂	4.30E-11	4.30E-11	(R. Sander et al., 2019)
<i>cab</i> ₁₃	CH ₃ OH + OH → 0.85 * HCHO +0.85 * HO ₂ + 0.15 * CH ₃ O + H ₂ O	6.38E-18(T ²)exp(144/T)	9.19E-13	(R. Sander et al., 2019)
<i>cab</i> ₁₄	CH ₃ OOH + OH → 0.6 * CH ₃ O ₂ +0.4 * HCHO + 0.4 * OH + H ₂ O	k.ch3ooh_oh	1.00E-11	(R. Sander et al., 2019)
<i>cab</i> ₁₅	CH ₃ O + O ₂ → HO ₂ + HCHO	1.30E-14exp(-633/T)	1.55E-15	(R. Sander et al., 2019)
<i>cab</i> ₁₆	CH ₃ O + O ₃ → CH ₃ O ₂ + O ₂	2.53E-14	2.53E-14	(R. Sander et al., 2019)
<i>cab</i> ₁₇	CH ₃ O + O → 0.75 * CH ₃ + 0.75 * O ₂ +0.25 * HCHO + 0.25 * OH	2.50e-11	2.50E-11	(R. Sander et al., 2019)
<i>cab</i> ₁₈	HCHO + OH → HCO + H ₂ O	5.50E-12exp(-125/T)	3.60e-12	(S. Sander et al., 2011)
<i>cab</i> ₁₉	HCHO + HO ₂ → HOCH ₂ O ₂	9.70E-15exp(625/T)	7.90E-14	(R. Sander et al., 2019)
<i>cab</i> ₂₀	HCHO + O → HCO + OH	2.99E-11exp(-1529/T)	1.77E-13	(Herron, 1988)
<i>cab</i> ₂₁	HCO + O → CO + OH	5.00E-11	5.00E-11	(Baulch et al., 1992)
<i>cab</i> ₂₂	HCO + CH ₃ → CH ₄ + CO	4.40E-11	4.40E-11	(S. Mulenko, 1987)
<i>cab</i> ₂₃	HCO + CH ₃ → CH ₃ CHO	4.42E-11	4.42E-11	(S. A. Mulenko, 1980)
<i>cab</i> ₂₄	HCO + HCO → HCHO + CO	4.48E-11	4.48E-11	(Friedrichs et al., 2002)
<i>cab</i> ₂₅	HCO + OH → CO + H ₂ O	1.69E-10	1.69E-10	(Baulch et al., 1992)
<i>cab</i> ₂₆	HCO + O ₂ → CO + HO ₂	5.20E-12	5.20E-12	(S. Sander et al., 2011)
<i>cab</i> ₂₇	HCO + H → CO + H ₂	1.83E-10	1.83E-10	(Friedrichs et al., 2002)
<i>cab</i> ₂₈	HOCH ₂ O ₂ → HCHO + HO ₂	2.40E12exp(-7000/T)	150.89 ^b	(R. Sander et al., 2019)
<i>cab</i> ₂₉	HOCH ₂ O ₂ + HO ₂ → 0.5 * HOCH ₂ OOH +0.5 * HCOOH + 0.2 * OH + 0.2 * HO ₂ + 0.3 * H ₂ O + 0.8 * O ₂	5.6E-15exp(2300/T)	1.26E-12	(R. Sander et al., 2019)
<i>cab</i> ₃₀	HOCH ₂ O ₂ + R - O ₂ → HCOOH + HO ₂	2 × (k.ch3o2 × 5.50E-12) ^{0.5}	2.78E-12	(R. Sander et al., 2019)
<i>cab</i> ₃₁	HOCH ₂ O ₂ + R - O ₂ → 0.5 * HCOOH +0.5 * HOCH ₂ OH + 0.5 * O ₂	2 × (k.ch3o2 × 5.70E-14 × exp(750/T)) ^{0.5}	9.95E-13	(R. Sander et al., 2019)
<i>cab</i> ₃₂	HCOOH + OH → CO ₂ + HO ₂ + H ₂ O	2.94E-14exp(786/T) + 9.85E-13exp(-1036/T)	4.42E-13	(R. Sander et al., 2019)
<i>cab</i> ₃₃	HOCH ₂ OOH + OH → HOCH ₂ O ₂	k.roohro	6.02E-12	(R. Sander et al., 2019)
<i>cab</i> ₃₄	HOCH ₂ OOH + OH → HCOOH + H ₂ O + OH	k.rohro + k.s × f.soh × f.sooH	2.59E-11	(R. Sander et al., 2019)
<i>cab</i> ₃₅	HOCH ₂ OH + OH → HO ₂ + HCOOH + H ₂ O	2 × k.rohro + k.s × f.soh ²	1.13E-11	(R. Sander et al., 2019)
<i>cab</i> ₁₀₇	CH ₃ + OH + M → CH ₃ OH + M	2.5 × dens × 2.48E-27exp(298./t) ^{3.8}	9.92E-10	(Fagerstrm et al., 1994)

Table B5. Chemical reactions and rate coefficients involved in the oxidation of C_2H_6 used in our 1-D photochemistry model. Bimolecular rate coefficient units are $cm^3 molec^{-1} s^{-1}$. ^a are three-body reactions with values taken with atmospheric number density complying to temperatures of $T = 298$ K and pressures of 660 Pa. ^b are unimolecular rate coefficients with units s^{-1} .

Ethane Reaction Scheme				
Key	Reaction	Formula	Rate at T = 298 K	Reference
cab36	$C_2H_6 + OH \rightarrow C_2H_5 + H_2O$	$7.66E-12 \exp(-1020/T)$	2.50E-13	(S. Sander et al., 2011)
cab37	$C_2H_6 + O \rightarrow C_2H_5 + OH$	$2.21E-15(T/298)^{0.5} \exp(-132/T)$	1.42E-15	(Cohen & Westberg, 1991)
cab38	$CH_3 + CH_3 + M \rightarrow C_2H_6$	Details in (Cody et al., 2003)	$5.12E-11^a$	(Cody et al., 2003)
cab39	$C_2H_5 + O_2 + M \rightarrow C_2H_5O_2$	$2.5 \times 1.50E-28(298/T)^3 \times \text{dens}$	$6.02E-11^a$	(S. Sander et al., 2011)
cab40	$C_2H_5 + C_2H_5 \rightarrow C_2H_4 + C_2H_6$	2.01E-12	2.01E-12	(Dobis & Benson, 1991)
cab41	$C_2H_5 + O_2 \rightarrow C_2H_4 + HO_2$	1.90E-14	1.90E-14	(S. Sander et al., 2011)
cab42	$C_2H_5 + H \rightarrow CH_3 + CH_3$	$7.95E-11 \exp(-132/T)$	5.11E-11	(Pratt & Wood, 1984)
cab43	$C_2H_5O_2 + HO_2 \rightarrow C_2H_5OOH + O_2$	$7.50E-13 \exp(700/T)$	7.86E-12	(R. Sander et al., 2019)
cab44	$C_2H_5O_2 + RO_2 \rightarrow 0.8 * CH_3CHO + 0.6 * HO_2 + 0.2 * C_2H_5OH + O_2$	$2(7.60E-14 * k_{ch3o2})^{0.5}$	3.27E-13	(R. Sander et al., 2019)
cab45	$C_2H_5OOH + HO_2 \rightarrow C_2H_5OOH + O_2$	k.roohro	6.02E-12	(R. Sander et al., 2019)
cab46	$C_2H_5OOH + OH \rightarrow CH_3CHO + OH$	k.s*f.sooh	7.47E-12	(R. Sander et al., 2019)
cab47	$C_2H_5OH + OH \rightarrow 0.95 * C_2H_5O_2 + 0.95 * HO_2 + 0.05 * HOCH_2CH_2O_2 + H_2O$	$3.00E-12 \exp(20/T)$	3.21E-12	(R. Sander et al., 2019)
cab48	$HOCH_2CH_2O_2 + RO_2 \rightarrow 0.6 * HOCH_2CH_2O + 0.2 * ETHGLY$	$2*(7.80E-14 \exp(1000/T) * k_{ch3o2})^{0.5}$	1.77E-12	(R. Sander et al., 2019)
cab49	$HOCH_2CH_2O_2 + HO_2 \rightarrow HYETHO_2H$	$1.53E-13 \exp(1300/T) * (1 - k_{rchohch2o2,oh})$	1.08E-11	(R. Sander et al., 2019)
cab50	$HOCH_2CH_2O_2 + HO_2 \rightarrow HOCH_2CH_2O + OH$	$1.53E-13 \exp(1300/T) * k_{rchohch2o2,oh}$	1.20E-12	(R. Sander et al., 2019)
cab51	$HOCH_2CH_2O + O_2 \rightarrow HO_2 + HOCH_2CHO$	$6.00E-14 \exp(-550/T)$	9.48E-15	(R. Sander et al., 2019)
cab52	$HOCH_2CH_2O \rightarrow HO_2 + HCHO + HCHO$	$9.5E13 \exp(-5988/T)$	1.78E ⁵	(R. Sander et al., 2019)
cab53	$ETHGLY + OH \rightarrow HOCH_2CHO + HO_2 + H_2O$	$2^*k_{s*f,soh*f,pc2oh} + 2^*k_{rohro}$	8.57E-12	(R. Sander et al., 2019)
cab54	$HYETHO_2H + OH \rightarrow HOCH_2CH_2O_2 + H_2O$	k.roohro	6.02E-12	(R. Sander et al., 2019)
cab55	$HYETHO_2H + OH \rightarrow HOCH_2CHO + OH + H_2O$	k.s*f.sooh*f,pc2oh	9.64E-12	(R. Sander et al., 2019)
cab56	$HYETHO_2H + OH \rightarrow HOOCH_2CHO + HO_2 + H_2O$	k.s*f,soh*f,pc2oh + k.rohro	4.29E-12	(R. Sander et al., 2019)
cab57	$CH_3CHO + OH \rightarrow CH_3C(O) + H_2O$	$4.40E-12 \exp(365/T) * 0.95$	1.42E-11	(R. Sander et al., 2019)
cab58	$CH_3CHO + OH \rightarrow HCOCH_2O_2 + H_2O$	$4.40E-12 \exp(365/T) * 0.05$	7.48E-13	(R. Sander et al., 2019)
cab59	$CH_3CHO + HO_2 \rightarrow CH_3CHOHO_2$	$3.46E12 \exp(-12500/(1.98*T)) / 6.34E26 * \exp(-1470/(1.98*T))$	4.77E-22	(R. Sander et al., 2019)
cab60	$CH_3CHO + HCOOH \rightarrow CH_3CHOH + HCOOH$	$(1.17E-19 * T^{2.209}) \exp(-556/(1.987T))$	1.34E-14	(R. Sander et al., 2019)
cab61	$CH_2CHOH + OH \rightarrow HCOOH + OH + HCHO$	4.30E-11	4.30E-11	(R. Sander et al., 2019)
cab62	$CH_2CHOH + OH \rightarrow HOCH_2CHO + HO_2$	2.40E-11	2.40E-11	(R. Sander et al., 2019)
cab63	$CH_2CHOH + HCOOH \rightarrow CH_3CHO + HCOOH$	$(4.67E-26 * T^{3.286}) \exp(-556/(T * 1.987))$	2.47E-18	(R. Sander et al., 2019)
cab64	$CH_3CHOHO_2 \rightarrow CH_3CHO + HO_2$	$3.46E12 \exp(-12500/(T * 1.98))$	2.18E ³	(R. Sander et al., 2019)
cab65	$CH_3CHOHO_2 + HO_2 \rightarrow 0.5 * CH_3CHOHOOH + 0.3 * CH_3COOH + 0.2 * CH_3 + 0.2 * HCOOH + 0.2 * OH + O_2$	5.60E-15 exp(2300/T)	1.26E-11	(R. Sander et al., 2019)
cab66	$CH_2CHOHO_2 + RO_2 \rightarrow CH_3 + HCOOH + OH$	k.ro2soro2	9.68E-13	(R. Sander et al., 2019)
cab67	$CH_2COOH + OH \rightarrow CH_3 + CO_2 + H_2O$	$4.00E-14 \exp(850/T)$	6.93E-13	(R. Sander et al., 2019)
cab68	$CH_2CHOHOHOH + OH \rightarrow CH_2COOH + OH$	k.t*f,toolh*f,foh + k.rohro	4.19E-11	(R. Sander et al., 2019)
cab69	$CH_2CHOHOHOH + OH \rightarrow CH_2CHOHO_2$	k.roohro	6.02E-12	(R. Sander et al., 2019)
cab70	$CH_3C(O) + O_2 + M \rightarrow CH_3C(O)OO + M$	$5.10E-12(1 - 1/(1 + 9.48E-18 * \text{dens} * 2.5))$	$4.04E-12^a$	(R. Sander et al., 2019)
cab71	$CH_3C(O) + O_2 + M \rightarrow OH + HCHO + CO + M$	$5.10E-12(1 + 9.48E-18 * \text{dens} * 2.5)$	$1.06E-12^a$	(R. Sander et al., 2019)
cab72	$CH_3C(O)OO + HO_2 \rightarrow OH + CH_3 + CO_2$	$5.20E-13 \exp(980/T) * 1.507 * 0.61$	1.28E-11	(R. Sander et al., 2019)
cab73	$CH_3C(O)OO + HO_2 \rightarrow CH_3C(O)OOH$	$5.20E-13 \exp(980/T) * 1.507 * 0.23$	4.83E-12	(R. Sander et al., 2019)
cab74	$CH_3C(O)OO + HO_2 \rightarrow CH_3COOH + O_3$	$5.20E-13 \exp(980/T) * 1.507 * 0.16$	3.36E-12	(R. Sander et al., 2019)
cab75	$CH_3C(O)OO + RO_2 \rightarrow CH_3 + CO_2$	k.ro2roo3*0.9	1.93E-11	(R. Sander et al., 2019)
cab76	$CH_3C(O)OO + RO_2 \rightarrow CH_3COOH$	k.ro2roo3*0.1	2.14E-12	(R. Sander et al., 2019)
cab77	$CH_3C(O)OOH + OH \rightarrow CH_3C(O)OO + H_2O$	k.roohro	6.02E-12	(R. Sander et al., 2019)
cab78	$HCOCH_2O_2 + RO_2 \rightarrow 0.6 * HCHO + 0.6 * CO + 0.6 * HO_2 + 0.2 * GLYOX + 0.2 * HOCH_2CHO$	k.ro2poro2	8.03E-12	(R. Sander et al., 2019)
cab79	$HCOCH_2O_2 + HO_2 \rightarrow HOOCH_2CHO$	k.ro2ho2,2*rcoch2o2,oo	7.52E-12	(R. Sander et al., 2019)
cab80	$HCOCH_2O_2 + HO_2 \rightarrow HCHO + CO + HO_2 + OH$	k.ro2ho2,2*rcoch2o2,oh	1.33E-12	(R. Sander et al., 2019)
cab81	$GLYOX + OH \rightarrow HCOCO + H_2O$	$3.10E-12 \exp(340/T)$	9.70E-12	(R. Sander et al., 2019)
cab82	$HCOCO \rightarrow HCO + CO$	$1.40E12 \exp(-3159/T)$	3.54E ⁷	(Orlando & Tyndall, 2001)
cab83	$HCOCO + O_2 \rightarrow HCOCO_3$	$5.00E-12 * 3.2^* \exp(-550/T)$	2.53E-12	(R. Sander et al., 2019)
cab84	$HCOCO + O_2 \rightarrow OH + CO + CO_2$	$5.00E-12(1 - 3.2 \exp(-550/T))$	2.47E-12	(R. Sander et al., 2019)
cab85	$HOOCH_2CHO + OH \rightarrow HCOCH_2O_2 + H_2O$	k.roohro	6.02E-12	(R. Sander et al., 2019)
cab86	$HOOCH_2CHO + OH \rightarrow HCHO + CO + OH + H_2O$	$0.8 * 8.00E-12$	6.40E-12	(R. Sander et al., 2019)
cab87	$HOOCH_2CHO + OH \rightarrow GLYOX + OH + H_2O$	$0.55 * k_{s*f,sooh*f,cho}$	2.26E-12	(R. Sander et al., 2019)
cab88	$HOCH_2CHO + OH \rightarrow HOCH_2CO + H_2O$	$0.8 * 8.00E-12$	6.40E-12	(R. Sander et al., 2019)
cab89	$HOCH_2CHO + OH \rightarrow HOCHCHO + H_2O$	$0.2 * 8.00E-12$	1.60E-12	(R. Sander et al., 2019)
cab90	$HOCHCHO \rightarrow GLYOX + HO_2$	kdec	1.00E ⁶	(R. Sander et al., 2019)
cab91	$HOCH_2CO + O_2 + M \rightarrow HOCH_2CO_3 + M$	$5.10E-12(1 - 1/(1 + 1.85E-18 * \text{dens} * 2.5))$	$2.17E-12^a$	(R. Sander et al., 2019)
cab92	$HOCH_2CO + O_2 + M \rightarrow OH + HCHO + CO_2 + M$	$5.10E-12(1 + 1.85E-18 * \text{dens} * 2.5)$	$8.89E-12^a$	(R. Sander et al., 2019)
cab93	$HOCH_2CO_3 + RO_2 \rightarrow HCHO + CO_2 + HO_2$	k.ro2roo3*0.9	1.93E-11	(R. Sander et al., 2019)
cab94	$HOCH_2CO_3 + RO_2 \rightarrow HOCH_2CO_2H$	k.ro2roo3*0.1	2.14E-12	(R. Sander et al., 2019)
cab95	$HOCH_2CO_3 + HO_2 \rightarrow HCHO + OH + HO_2 + CO_2$	kapho2*rco3,oh	9.25E-12	(R. Sander et al., 2019)
cab96	$HOCH_2CO_3 + HO_2 \rightarrow HOCH_2CO_3H$	kapho2*rco3,oo	2.82E-12	(R. Sander et al., 2019)
cab97	$HOCH_2CO_3 + HO_2 \rightarrow HOCH_2CO_2H + O_3$	kapho2*rco3,oo	1.34E-12	(R. Sander et al., 2019)
cab98	$HOCH_2CO_2H + OH \rightarrow 0.09 * HCHO + 0.91 * HCOCO_2H + HO_2 + H_2O$	k.co2h + k.s*f,soh*f,co2h	5.50E012	(R. Sander et al., 2019)
cab99	$HCOCO_2H + OH \rightarrow CO + HO_2 + CO_2 + H_2O$	k.co2h + k.t*f,co*f,co2h	2.66E-11	(R. Sander et al., 2019)
cab100	$HOCH_2CO_2H + OH \rightarrow HOCH_2CO_3 + H_2O$	k.roohro	6.02E-12	(R. Sander et al., 2019)
cab101	$HOCH_2CO_2H + OH \rightarrow HCOCO_2H + HO_2$	k.s*f,soh*f,co2h	5.37E-12	(R. Sander et al., 2019)
cab102	$HCOCO_2H + OH \rightarrow HCOCO_3 + H_2O$	k.roohro	6.02E-12	(R. Sander et al., 2019)
cab103	$HCOCO_2H + OH \rightarrow CO + CO_2 + H_2O + OH$	k.t*f,co*f,co2h	2.65E-11	(R. Sander et al., 2019)
cab104	$HCOCO_3 + RO_2 \rightarrow CO + HO_2 + CO_2$	k.ro2roo3*0.9	1.93E-11	(R. Sander et al., 2019)
cab105	$HCOCO_3 + RO_2 \rightarrow HCOCO_2H + O_2$	k.ro2roo3*0.1	2.14E-12	(R. Sander et al., 2019)
cab106	$HCOCO_3 + HO_2 \rightarrow HO_2 + CO + CO_2 + OH$	kapho2	1.34E-11	(R. Sander et al., 2019)

Table B6. Organic photolytic reactions used within the 1-D photochemistry submodule. Values (s^{-1}) are interpolated from an offline look-up table constructed by a modified TUV (Madronich et al., 2002) model with respect to CO_2 and O_3 column abundances overhead, temperature, optical opacity and solar zenith angle. Values displayed are extracted for a solar zenith angle of 0° , $L_S = 251^\circ$ (perihelion).

Key	Reaction	$J(z = 0.50 \text{ km})$	$J(z = 42.67 \text{ km})$	$J(z = 69.81 \text{ km})$
$j_{CH_4 \rightarrow CH_3}$	$CH_4 + h\nu \rightarrow CH_3 + H$	0.00	0.00	8.12E-10
$j_{CH_4 \rightarrow ^1CH_2}$	$CH_4 + h\nu \rightarrow ^1CH_2 + H_2$	0.00	0.00	1.63E-9
$j_{CH_4 \rightarrow ^3CH_2}$	$CH_4 + h\nu \rightarrow ^3CH_2 + H + H$	0.00	0.00	1.53E-10
$j_{CH_4 \rightarrow CH}$	$CH_4 + h\nu \rightarrow CH + H_2 + H$	0.00	0.00	1.95E-10
j_{CH_3OOH}	$CH_3OOH + h\nu \rightarrow CH_3O + OH$	2.23E-5	2.90E-5	2.97E-5
$j_{HCHO \rightarrow HCO}$	$HCHO + h\nu \rightarrow HCO + H$	3.54E-5	4.62E-5	4.74E-5
$j_{HCHO \rightarrow CO}$	$HCHO + h\nu \rightarrow H_2 + CO$	3.71E-5	4.88E-5	5.01E-5
j_{CH_3OH}	$CH_3OH + h\nu \rightarrow CH_3O + H$	1.59E-7	1.12E-6	1.64E-6
$j_{C_2H_6}$	$C_2H_6 + h\nu \rightarrow \text{Products}$	0.00	0.00	2.39E-9
$j_{CH_3CHO \rightarrow CH_3}$	$CH_3CHO + h\nu \rightarrow CH_3 + HCO$	2.43E-5	3.40E-5	3.44E-5
$j_{CH_3CHO \rightarrow CH_4}$	$CH_3CHO + h\nu \rightarrow CH_4 + CO$	5.46E-6	6.80E-6	6.81E-6
j_{HOCH_2OOH}	$HOCH_2OOH + h\nu(+O_2) \rightarrow HCOOH + HO_2 + OH$	4.43E-5	5.43E-5	5.43E-5
$j_{HOCH_2CHO \rightarrow HCO}$	$HOCH_2CHO + h\nu \rightarrow CH_3O + HCO$	4.08E-5	5.04E-5	5.05E-5
$j_{HOCH_2CHO \rightarrow CO}$	$HOCH_2CHO + h\nu \rightarrow CH_3OH + CO$	4.91E-6	6.07E-6	6.09E-6
$j_{HOCH_2CHO \rightarrow OH}$	$HOCH_2CHO + h\nu(+O_2) \rightarrow HCOCH_2O_2 + OH$	3.44E-6	4.25E-6	4.26E-6
$j_{Glyox \rightarrow HCO}$	$Glyoxal + h\nu \rightarrow HCO + HCO$	7.84E-5	8.49E-5	8.5E-5
$j_{Glyox \rightarrow H_2}$	$Glyoxal + h\nu \rightarrow H_2 + CO + CO$	1.90E-5	2.19E-5	2.20E-5
$j_{Glyox \rightarrow HCHO}$	$Glyoxal + h\nu \rightarrow HCHO + CO$	2.79E-5	3.13E-5	3.14E-5
j_{CH_3COOH}	$CH_3COOH + h\nu \rightarrow CH_3 + COOH$	7.77E-6	9.43E-6	9.44E-6
$j_{CH_3C(O)OOH}$	$CH_3C(O)OOH + h\nu \rightarrow CH_3 + OH + CO_2$	3.85E-5	4.73E-6	4.75E-5
Proxies				
Key	Reaction	Proxy	Source	
$j_{HOCH_2CO_3H}$	$HOCH_2CO_3H + h\nu \rightarrow HCHO + HO_2 + OH + CO_2$	j_{CH_3OOH}	(R. Sander et al., 2014)	
j_{HCOCO_2H}	$HCOCO_2H + h\nu \rightarrow 2HO_2 + CO + CO_2$	$3.95 \times j_{HCHO \rightarrow CO}$	(Kuhlmann et al., 2003)	
$j_{CH_3CHOHOOH}$	$CH_3CHOHOOH + h\nu \rightarrow CH_3 + HCOOH + OH$	j_{CH_3OOH}	(R. Sander et al., 2014)	
$j_{Hyetho2h}$	$Hyetho2h + h\nu \rightarrow HO_2 + CO + OH + CO_2$	$j_{CH_3OOH} + j_{HOCH_2CHO \rightarrow HCO} + j_{HOCH_2CHO \rightarrow CO} + j_{HOCH_2CHO \rightarrow OH}$	(R. Sander et al., 2014)	
j_{HCOCO_3H}	$HCOCO_3H + h\nu \rightarrow HO_2 + CO + OH + CO_2$	$j_{Hyetho2h}$	(R. Sander et al., 2014)	
j_{HOCH_2CHO}	$HOCH_2CHO + h\nu \rightarrow HCHO + OH + HO_2 + CO$	$j_{Hyetho2h}$	(R. Sander et al., 2014)	

- 681 R. G., ... Subcommittee, I. (2006). Evaluated kinetic and photochem-
 682 ical data for atmospheric chemistry: Volume ii; gas phase reactions of or-
 683 ganic species. *Atmospheric Chemistry and Physics*, 6(11), 3625–4055. Re-
 684 trieved from <https://www.atmos-chem-phys.net/6/3625/2006/> doi:
 685 10.5194/acp-6-3625-2006
- 686 Baulch, D. L., Bowman, C. T., Cobos, C. J., Cox, R. A., Just, T., Kerr, J. A., ...
 687 Warnatz, J. (2005). Evaluated kinetic data for combustion modeling: Supple-
 688 ment ii. *Journal of Physical and Chemical Reference Data*, 34(3), 757-1397.
 689 doi: 10.1063/1.1748524
- 690 Baulch, D. L., Cobos, C. J., Cox, R. A., Esser, C., Frank, P., Just, T., ... War-
 691 natz, J. (1992). Evaluated kinetic data for combustion modelling. *Journal*
 692 *of Physical and Chemical Reference Data*, 21(3), 411-734. Retrieved from
 693 <https://doi.org/10.1063/1.555908> doi: 10.1063/1.555908
- 694 Campbell, I., & Gray, C. (1973). Rate constants for o(3p) recombination and associ-
 695 ation with n(4s). *Chemical Physics Letters*, 18(4), 607 - 609. doi: [https://doi](https://doi.org/10.1016/0009-2614(73)80479-8)
 696 [.org/10.1016/0009-2614\(73\)80479-8](https://doi.org/10.1016/0009-2614(73)80479-8)
- 697 Christensen, L. E., Okumura, M., Sander, S. P., Salawitch, R. J., Toon, G. C., Sen,
 698 B., ... Jucks, K. W. (2002). Kinetics of ho2 + ho2 h2o2 + o2: Implications
 699 for stratospheric h2o2. *Geophysical Research Letters*, 29(9), 13-1-13-4. doi:
 700 10.1029/2001GL014525
- 701 Cody, R. J., Romani, P. N., Nesbitt, F. L., Iannone, M. A., Tardy, D. C., & Stief,
 702 L. J. (2003). Rate constant for the reaction ch3 + ch3 c2h6 at t = 155 k
 703 and model calculation of the ch3 abundance in the atmospheres of saturn and
 704 neptune. *Journal of Geophysical Research: Planets*, 108(E11). Retrieved
 705 from [https://agupubs.onlinelibrary.wiley.com/doi/abs/10.1029/](https://agupubs.onlinelibrary.wiley.com/doi/abs/10.1029/2002JE002037)
 706 [2002JE002037](https://agupubs.onlinelibrary.wiley.com/doi/abs/10.1029/2002JE002037) doi: 10.1029/2002JE002037
- 707 Cohen, N., & Westberg, K. R. (1991). Chemical kinetic data sheets for hightem-
 708 perature reactions. part ii. *Journal of Physical and Chemical Reference Data*,
 709 20(6), 1211-1311. Retrieved from <https://doi.org/10.1063/1.555901> doi:
 710 10.1063/1.555901
- 711 Dobis, O., & Benson, S. W. (1991). Temperature coefficients of the rates of chlorine
 712 atom reactions with c2h6, c2h5, and c2h4. the rates of disproportionation and
 713 recombination of ethyl radicals. *Journal of the American Chemical Society*,
 714 113(17), 6377-6386. Retrieved from <https://doi.org/10.1021/ja00017a004>
 715 doi: 10.1021/ja00017a004
- 716 Fagerstrm, K., Lund, A., Mahmoud, G., Jodkowski, J. T., & Ratajczak, E. (1994).
 717 Pressure and temperature dependence of the gas-phase reaction between
 718 methyl and hydroxyl radicals. *Chemical Physics Letters*, 224(1), 43 - 50.
 719 Retrieved from [http://www.sciencedirect.com/science/article/pii/](http://www.sciencedirect.com/science/article/pii/0009261494005133)
 720 [0009261494005133](http://www.sciencedirect.com/science/article/pii/0009261494005133) doi: [https://doi.org/10.1016/0009-2614\(94\)00513-3](https://doi.org/10.1016/0009-2614(94)00513-3)
- 721 Fedorova, A., Korablev, O., Bertaux, J.-L., Rodin, A., Kiselev, A., & Perrier, S.
 722 (2006). Mars water vapor abundance from spicam ir spectrometer: Seasonal
 723 and geographic distributions. *Journal of Geophysical Research: Planets*,
 724 111(E9). Retrieved from [https://agupubs.onlinelibrary.wiley.com/doi/](https://agupubs.onlinelibrary.wiley.com/doi/abs/10.1029/2006JE002695)
 725 [abs/10.1029/2006JE002695](https://agupubs.onlinelibrary.wiley.com/doi/abs/10.1029/2006JE002695) doi: 10.1029/2006JE002695
- 726 Fonti, S., & Marzo, G. A. (2010, Mar). Mapping the methane on Mars. *Astronomy*
 727 *and Astrophysics*, 512, A51. doi: 10.1051/0004-6361/200913178
- 728 Forget, F., Hourdin, F., Fournier, R., Hourdin, C., Talagrand, O., Collins, M., ...
 729 Huot, J.-P. (1999, October). Improved general circulation models of the
 730 Martian atmosphere from the surface to above 80 km. *Journal of Geophysics*
 731 *Research*, 104, 24155-24176. doi: 10.1029/1999JE001025
- 732 Forget, F., Hourdin, F., & Talagrand, O. (1998, February). CO₂ Snowfall on Mars:
 733 Simulation with a General Circulation Model. *Icarus*, 131, 302-316. doi: 10
 734 [.1006/icar.1997.5874](https://doi.org/10.1006/icar.1997.5874)
- 735 Formisano, V., Angrilli, F., Arnold, G., Atreya, S., Bianchini, G., Biondi, D.,

- 736 ... Zasova, L. (2005). The planetary fourier spectrometer (pfs) on-
 737 board the european mars express mission. *Planetary and Space Science*,
 738 53(10), 963 - 974. Retrieved from [http://www.sciencedirect.com/](http://www.sciencedirect.com/science/article/pii/S0032063305000644)
 739 [science/article/pii/S0032063305000644](http://www.sciencedirect.com/science/article/pii/S0032063305000644) (First Results of the Plan-
 740 etary Fourier Spectrometer aboard the the Mars Express Mission) doi:
 741 <https://doi.org/10.1016/j.pss.2004.12.006>
- 742 Formisano, V., Atreya, S., Encrenaz, T., Ignatiev, N., & Giuranna, M. (2004). De-
 743 tecton of methane in the atmosphere of mars. *Science*, 306(5702), 1758–1761.
 744 Retrieved from <http://science.sciencemag.org/content/306/5702/1758>
 745 doi: 10.1126/science.1101732
- 746 Friedrichs, G., Herbon, J. T., Davidson, D. F., & Hanson, R. K. (2002). Quan-
 747 titative detection of hco behind shock waves: The thermal decomposi-
 748 tion of hco. *Phys. Chem. Chem. Phys.*, 4, 5778-5788. Retrieved from
 749 <http://dx.doi.org/10.1039/B205692E> doi: 10.1039/B205692E
- 750 Geminale, A., Formisano, V., & Giuranna, M. (2008). Methane in martian
 751 atmosphere: Average spatial, diurnal, and seasonal behaviour. *Plan-*
 752 *etary and Space Science*, 56(9), 1194 - 1203. Retrieved from [http://](http://www.sciencedirect.com/science/article/pii/S0032063308000743)
 753 www.sciencedirect.com/science/article/pii/S0032063308000743 doi:
 754 <https://doi.org/10.1016/j.pss.2008.03.004>
- 755 Geminale, A., Formisano, V., & Sindoni, G. (2011). Mapping methane in mar-
 756 tian atmosphere with pfs-mex data. *Planetary and Space Science*, 59(2), 137 -
 757 148. Retrieved from [http://www.sciencedirect.com/science/article/pii/](http://www.sciencedirect.com/science/article/pii/S0032063310002138)
 758 [S0032063310002138](http://www.sciencedirect.com/science/article/pii/S0032063310002138) (Methane on Mars: Current Observations, Interpretation
 759 and Future Plans) doi: <https://doi.org/10.1016/j.pss.2010.07.011>
- 760 Giuranna, M., Viscardy, S., Daerden, F., Neary, L., Etiope, G., Oehler, D., ...
 761 Amoroso, M. (2019). Independent confirmation of a methane spike on
 762 mars and a source region east of gale crater. *Nature Geoscience*. Re-
 763 trieved from <https://doi.org/10.1038/s41561-019-0331-9> doi:
 764 10.1038/s41561-019-0331-9
- 765 Gordon, I., Rothman, L., Hill, C., Kochanov, R., Tan, Y., Bernath, P., ... Zak,
 766 E. (2017). The hitran2016 molecular spectroscopic database. *Journal of*
 767 *Quantitative Spectroscopy and Radiative Transfer*, 203, 3 - 69. Retrieved from
 768 <http://www.sciencedirect.com/science/article/pii/S0022407317301073>
 769 (HITRAN2016 Special Issue) doi: <https://doi.org/10.1016/j.jqsrt.2017.06.038>
- 770 Groß, C. B. M., Dillon, T. J., Schuster, G., Lelieveld, J., & Crowley, J. N. (2014).
 771 Direct kinetic study of oh and o3 formation in the reaction of ch3c(o)o2 with
 772 ho2. *The Journal of Physical Chemistry A*, 118(6), 974-985. Retrieved
 773 from <https://doi.org/10.1021/jp412380z> (PMID: 24491030) doi:
 774 10.1021/jp412380z
- 775 Guenther, A., Geron, C., Pierce, T., Lamb, B., Harley, P., & Fall, R. (2000). Nat-
 776 ural emissions of non-methane volatile organic compounds, carbon monox-
 777 ide, and oxides of nitrogen from north america. *Atmospheric Environment*,
 778 34(12), 2205 - 2230. Retrieved from [http://www.sciencedirect.com/](http://www.sciencedirect.com/science/article/pii/S1352231099004653)
 779 [science/article/pii/S1352231099004653](http://www.sciencedirect.com/science/article/pii/S1352231099004653) doi: [https://doi.org/10.1016/](https://doi.org/10.1016/S1352-2310(99)00465-3)
 780 [S1352-2310\(99\)00465-3](https://doi.org/10.1016/S1352-2310(99)00465-3)
- 781 Herron, J. T. (1988). Evaluated chemical kinetic data for the reactions of atomic
 782 oxygen o(3p) with saturated organic compounds in the gas phase. *Journal*
 783 *of Physical and Chemical Reference Data*, 17(3), 967-1026. Retrieved from
 784 <https://doi.org/10.1063/1.555810> doi: 10.1063/1.555810
- 785 Horita, J., & Berndt, M. E. (1999). Abiogenic methane formation and isotopic
 786 fractionation under hydrothermal conditions. *Science*, 285(5430), 1055–1057.
 787 Retrieved from <https://science.sciencemag.org/content/285/5430/1055>
 788 doi: 10.1126/science.285.5430.1055
- 789 Joshi, A. V., & Wang, H. (2006). Master equation modeling of wide range temper-
 790 ature and pressure dependence of co + oh products. *International Journal of*

- 791 *Chemical Kinetics*, 38(1), 57-73. doi: 10.1002/kin.20137
- 792 Kaufman, F., & Kelso, J. R. (1967). M effect in the gasphase recombination of o
793 with o2. *The Journal of Chemical Physics*, 46(11), 4541-4543. Retrieved from
794 <https://doi.org/10.1063/1.1840589> doi: 10.1063/1.1840589
- 795 Korablev, O., Montmessin, F., Trokhimovskiy, A., Fedorova, A. A., Shakun, A. V.,
796 Grigoriev, A. V., ... Zorzano, M. P. (2017, Nov 30). The atmospheric chem-
797 istry suite (acs) of three spectrometers for the exomars 2016 trace gas orbiter.
798 *Space Science Reviews*, 214(1), 7. Retrieved from [https://doi.org/10.1007/
799 s11214-017-0437-6](https://doi.org/10.1007/s11214-017-0437-6) doi: 10.1007/s11214-017-0437-6
- 800 Korablev, O., Vandaele, A. C., Montmessin, F., Fedorova, A. A., Trokhimovskiy,
801 A., Forget, F., ... Zorzano, M. P. (2019, Apr). No detection of methane on
802 Mars from early ExoMars Trace Gas Orbiter observations. *Nature*, 568(7753),
803 517-520. doi: 10.1038/s41586-019-1096-4
- 804 Krasnopolsky, V., Bjoraker, G., Mumma, M., & Jennings, D. (1997). High-
805 resolution spectroscopy of mars at 3.7 and 8 m: A sensitive search for h2o2,
806 h2co, hcl, and ch4, and detection of hdo. *Journal of Geophysical Research*
807 *E: Planets*, 102(E3), 6525-6534. Retrieved from [https://www.scopus
808 .com/inward/record.uri?eid=2-s2.0-17044428646&doi=10.1029%
809 2f96JE03766&partnerID=40&md5=4e1eeef318f69e58131c27b14599b572](https://www.scopus.com/inward/record.uri?eid=2-s2.0-17044428646&doi=10.1029%2f96JE03766&partnerID=40&md5=4e1eeef318f69e58131c27b14599b572)
810 (cited By 118) doi: 10.1029/96JE03766
- 811 Krasnopolsky, V. A. (2006). Some problems related to the origin of methane on
812 mars. *Icarus*, 180(2), 359 - 367. Retrieved from [http://www.sciencedirect
813 .com/science/article/pii/S0019103505004161](http://www.sciencedirect.com/science/article/pii/S0019103505004161) doi: [https://doi.org/
814 10.1016/j.icarus.2005.10.015](https://doi.org/10.1016/j.icarus.2005.10.015)
- 815 Krasnopolsky, V. A. (2007). Long-term spectroscopic observations of mars using
816 irtf/cshell: Mapping of o2 dayglow, co, and search for ch4. *Icarus*, 190(1), 93 -
817 102. Retrieved from [http://www.sciencedirect.com/science/article/pii/
818 S0019103507001005](http://www.sciencedirect.com/science/article/pii/S0019103507001005) doi: <https://doi.org/10.1016/j.icarus.2007.02.014>
- 819 Krasnopolsky, V. A. (2011, October). A Sensitive Search for Methane and Ethane
820 on Mars. In *Epsc-dps joint meeting 2011* (p. 49).
- 821 Krasnopolsky, V. A. (2012). Search for methane and upper limits to ethane
822 and so2 on mars. *Icarus*, 217(1), 144 - 152. Retrieved from [http://
823 www.sciencedirect.com/science/article/pii/S001910351100412X](http://www.sciencedirect.com/science/article/pii/S001910351100412X) doi:
824 <https://doi.org/10.1016/j.icarus.2011.10.019>
- 825 Krasnopolsky, V. A., Maillard, J. P., & Owen, T. C. (2004). Detection of methane
826 in the martian atmosphere: evidence for life? *Icarus*, 172(2), 537 - 547.
827 Retrieved from [http://www.sciencedirect.com/science/article/pii/
828 S0019103504002222](http://www.sciencedirect.com/science/article/pii/S0019103504002222) doi: <https://doi.org/10.1016/j.icarus.2004.07.004>
- 829 Kuhlmann, R., Lawrence, M., Crutzen, P., & Rasch, P. (2003, 05). A model for
830 studies of tropospheric ozone and nonmethane hydrocarbons: Model descrip-
831 tion and ozone results. *Journal of Geophysical Research*, v.108 (2003), 108.
832 doi: 10.1029/2002JD002893
- 833 Lefèvre, F., & Forget, F. (2009). Observed variations of methane on mars unex-
834 plained by known atmospheric chemistry and physics. *Nature*, 460, 720. doi:
835 10.1038/nature08228
- 836 Lefèvre, F., Lebonnois, S., Montmessin, F., & Forget, F. (2004). Three-dimensional
837 modeling of ozone on mars. *Journal of Geophysical Research: Planets*,
838 109(E7). Retrieved from [https://agupubs.onlinelibrary.wiley.com/
839 doi/abs/10.1029/2004JE002268](https://agupubs.onlinelibrary.wiley.com/doi/abs/10.1029/2004JE002268) doi: 10.1029/2004JE002268
- 840 Lewis, S. R., Collins, M., Read, P. L., Forget, F., Hourdin, F., Fournier, R., ...
841 Huot, J.-P. (1999). A climate database for mars. *Journal of Geophysi-
842 cal Research: Planets*, 104(E10), 24177-24194. Retrieved from [https://
843 agupubs.onlinelibrary.wiley.com/doi/abs/10.1029/1999JE001024](https://agupubs.onlinelibrary.wiley.com/doi/abs/10.1029/1999JE001024) doi:
844 10.1029/1999JE001024
- 845 Madeleine, J.-B., Forget, F., Millour, E., Montabone, L., & Wolff, M. J. (2011,

- 846 November). Revisiting the radiative impact of dust on Mars using the LMD
 847 Global Climate Model. *Journal of Geophysical Research (Planets)*, *116*,
 848 E11010. doi: 10.1029/2011JE003855
- 849 Madronich, S., Flocke, S., Zeng, J., Petropavlovskikh, I., & Lee-Taylor, J. (2002).
 850 Tropospheric ultraviolet and visible (tuv) radiation model. *National Center for*
 851 *Atmospheric Research (NCAR), Boulder, CO. Home page at: [http://www.acd.](http://www.acd.ucar.edu/TUV)*
 852 *ucar.edu/TUV*.
- 853 Mellor, G. L., & Yamada, T. (1982, November). Development of a turbulence clo-
 854 sure model for geophysical fluid problems. *Reviews of Geophysics and Space*
 855 *Physics*, *20*, 851-875. doi: 10.1029/RG020i004p00851
- 856 Millour, E., Forget, F., Spiga, A., Vals, M., Zakharov, V., Navarro, T., ...
 857 MCD/GCM Development Team (2017, April). The Mars Climate Database
 858 (MCD version 5.3). In *Egu general assembly conference abstracts* (Vol. 19,
 859 p. 12247).
- 860 Montabone, L., Forget, F., Millour, E., Wilson, R., Lewis, S., Cantor, B., ...
 861 Wolff, M. (2015). Eight-year climatology of dust optical depth on mars.
 862 *Icarus*, *251*, 65 - 95. Retrieved from [http://www.sciencedirect.com/](http://www.sciencedirect.com/science/article/pii/S0019103515000044)
 863 [science/article/pii/S0019103515000044](http://www.sciencedirect.com/science/article/pii/S0019103515000044) (Dynamic Mars) doi:
 864 <https://doi.org/10.1016/j.icarus.2014.12.034>
- 865 Moores, J. E., King, P. L., Smith, C. L., Martinez, G. M., Newman, C. E.,
 866 Guzewich, S. D., ... Schuerger, A. C. (2019). The methane diurnal variation
 867 and microseepage flux at gale crater, mars as constrained by the exomars trace
 868 gas orbiter and curiosity observations. *Geophysical Research Letters*, *46*(16),
 869 9430-9438. Retrieved from [https://agupubs.onlinelibrary.wiley.com/](https://agupubs.onlinelibrary.wiley.com/doi/abs/10.1029/2019GL083800)
 870 [doi/abs/10.1029/2019GL083800](https://agupubs.onlinelibrary.wiley.com/doi/abs/10.1029/2019GL083800) doi: 10.1029/2019GL083800
- 871 Mulenko, S. (1987). The application of an intracavity laser spectroscopy method
 872 for elementary processes study in gas-phase reactions. *Revue Roumaine de*
 873 *Physique*.
- 874 Mulenko, S. A. (1980). Investigation of the recombination of the hco radical in
 875 an atmosphere of argon and helium by the method of internal resonator laser
 876 spectroscopy. *Journal of Applied Spectroscopy*, *33*, 688-694.
- 877 Mumma, M. J., Villanueva, G. L., Novak, R. E., Hewagama, T., Bonev, B. P.,
 878 DiSanti, M. A., ... Smith, M. D. (2009). Strong release of methane on
 879 mars in northern summer 2003. *Science*, *323*(5917), 1041-1045. Retrieved
 880 from <http://science.sciencemag.org/content/323/5917/1041> doi:
 881 [10.1126/science.1165243](https://doi.org/10.1126/science.1165243)
- 882 Nair, H., Allen, M., Anbar, A. D., Yung, Y. L., & Clancy, R. T. (1994). A pho-
 883 tochemical model of the martian atmosphere. *Icarus*, *111*(1), 124 - 150.
 884 Retrieved from [http://www.sciencedirect.com/science/article/pii/](http://www.sciencedirect.com/science/article/pii/S0019103584711377)
 885 [S0019103584711377](http://www.sciencedirect.com/science/article/pii/S0019103584711377) doi: <https://doi.org/10.1006/icar.1994.1137>
- 886 Navarro, T., Madeleine, J.-B., Forget, F., Spiga, A., Millour, E., Montmessin, F.,
 887 & Määttänen, A. (2014, July). Global climate modeling of the Martian
 888 water cycle with improved microphysics and radiatively active water ice
 889 clouds. *Journal of Geophysical Research (Planets)*, *119*, 1479-1495. doi:
 890 [10.1002/2013JE004550](https://doi.org/10.1002/2013JE004550)
- 891 Orlando, J. J., & Tyndall, G. S. (2001). The atmospheric chemistry of the
 892 hc(o)co radical. *International Journal of Chemical Kinetics*, *33*(3), 149-
 893 156. Retrieved from [https://onlinelibrary.wiley.com/doi/abs/10.1002/](https://onlinelibrary.wiley.com/doi/abs/10.1002/1097-4601(200103)33:3<149::AID-KIN1008>3.0.CO;2-1)
 894 [1097-4601\(200103\)33:3<149::AID-KIN1008>3.0.CO;2-1](https://onlinelibrary.wiley.com/doi/abs/10.1002/1097-4601(200103)33:3<149::AID-KIN1008>3.0.CO;2-1)
 895 doi: 10.1002/1097-4601(200103)33:3<149::AID-KIN1008>3.0.CO;2-1
- 896 Pratt, G. L., & Wood, S. W. (1984). Kinetics of the reaction of methyl radicals
 897 with oxygen. *J. Chem. Soc., Faraday Trans. 1*, *80*, 3419-3427. Retrieved from
 898 <http://dx.doi.org/10.1039/F19848003419> doi: 10.1039/F19848003419
- 899 Robert, S., Vandaele, A., Thomas, I., Willame, Y., Daerden, F., Delanoye, S., ...
 900 Bellucci, G. (2016). Expected performances of the nomad/exomars in-

- 901 strument. *Planetary and Space Science*, 124, 94 - 104. Retrieved from
 902 <http://www.sciencedirect.com/science/article/pii/S0032063315301203>
 903 doi: <https://doi.org/10.1016/j.pss.2016.03.003>
- 904 Rodrigo, R., Garca-Ivarez, E., Lpez-Gonzlez, M. J., & Lpez-Moreno, J. J. (1990).
 905 A nonsteady one-dimensional theoretical model of mars' neutral atmo-
 906 spheric composition between 30 and 200 km. *Journal of Geophysical Re-*
 907 *search: Solid Earth*, 95(B9), 14795-14810. Retrieved from [https://](https://agupubs.onlinelibrary.wiley.com/doi/abs/10.1029/JB095iB09p14795)
 908 agupubs.onlinelibrary.wiley.com/doi/abs/10.1029/JB095iB09p14795
 909 doi: 10.1029/JB095iB09p14795
- 910 Rosner, B. M., & Schink, B. (1995, 11). Purification and characterization of acety-
 911 lene hydratase of pelobacter acetylenicus, a tungsten iron-sulfur protein. *Jour-*
 912 *nal of bacteriology*, 177, 5767-72. doi: 10.1128/jb.177.20.5767-5772.1995
- 913 Sander, R., Baumgaertner, A., Cabrera-Perez, D., Frank, F., Gromov, S., Grooß,
 914 J.-U., ... Tauer, S. (2019). The community atmospheric chemistry box model
 915 caaba/mecca-4.0. *Geoscientific Model Development*, 12(4), 1365–1385. Re-
 916 trieved from <https://www.geosci-model-dev.net/12/1365/2019/> doi:
 917 10.5194/gmd-12-1365-2019
- 918 Sander, R., Jckel, P., Kirner, O., Kunert, A., Landgraf, J., Pozzer, A., & Kirner, O.
 919 (2014, 11). The photolysis module jval-14, compatible with the messy stan-
 920 dard, and the jval preprocessor (jvpp). *Geoscientific Model Development*, 7,
 921 2653-2662. doi: 10.5194/gmd-7-2653-2014
- 922 Sander, S., Abbatt, J., Barker, J., Burkholder, J., Friedl, R., Golden, D., ... Wine,
 923 P. (2011, 06). Chemical kinetics and photochemical data for use in atmo-
 924 spheric studies, evaluation no. 17.
- 925 Sander, S., Finlayson-Pitts, B., Friedl, R., Golden, D., Huie, R., Keller-Rudek, H.,
 926 ... Wine, P. (2006, 01). Chemical kinetics and photochemical data for use in
 927 atmospheric studies. evaluation no. 15 (jpl publication 06-2).
- 928 Sander, S., Friedl, R., Golden, D., Kurylo, M., Huie, R., Orkin, V., ... Finlayson-
 929 Pitts, B. (2003, 01). Chemical kinetics and photochemical data for use in
 930 atmospheric studies; jpl publication 02-25.
- 931 Summers, M. E., Lieb, J. B., Chapman, E., & Yung, Y. L. (2002). Atmospheric
 932 biomarkers of subsurface life on mars. *Geophysical Research Letters*, 29(24),
 933 24-1-24-4. Retrieved from [https://agupubs.onlinelibrary.wiley.com/doi/](https://agupubs.onlinelibrary.wiley.com/doi/abs/10.1029/2002GL015377)
 934 [abs/10.1029/2002GL015377](https://agupubs.onlinelibrary.wiley.com/doi/abs/10.1029/2002GL015377) doi: 10.1029/2002GL015377
- 935 Taraborrelli, D. (2010). *Isoprene oxidation and its impacts on the atmospheric*
 936 *composition* (Doctoral dissertation, Johannes Gutenberg-Universität, Mainz,
 937 Germany). Retrieved from <http://d-nb.info/1003538770/34>
- 938 Taysum, B. (2020a, May). *bentaysum/1D_model_rebuild: Revised: AGU - Pho-*
 939 *tochemistry of Methane and Ethane in the Martian Atmosphere*. Zen-
 940 odo. Retrieved from <https://doi.org/10.5281/zenodo.3824053> doi:
 941 10.5281/zenodo.3824053
- 942 Taysum, B. (2020b, March). *Datafiles for the 1-d photochemistry submodule*. Zen-
 943 odo. Retrieved from <https://doi.org/10.5281/zenodo.3733208> doi: 10
 944 .5281/zenodo.3733208
- 945 Taysum, B. (2020c, March). *Output Files of the 1-D Submodule in The Pho-*
 946 *tochemistry of Methane and Ethane in the Martian Atmosphere*. Zen-
 947 odo. Retrieved from <https://doi.org/10.5281/zenodo.3824085> doi:
 948 10.5281/zenodo.3824085
- 949 Tsang, W., & Hampson, R. F. (1986). Chemical kinetic data base for combustion
 950 chemistry. part i. methane and related compounds. *Journal of Physical and*
 951 *Chemical Reference Data*, 15(3), 1087-1279. doi: 10.1063/1.555759
- 952 Vago, J., Witasse, O., Svedhem, H., Baglioni, P., Haldemann, A., Gianfiglio, G., ...
 953 de Groot, R. (2015, Dec 01). Esa exomars program: The next step in explor-
 954 ing mars. *Solar System Research*, 49(7), 518–528. Retrieved from [https://](https://doi.org/10.1134/S0038094615070199)
 955 doi.org/10.1134/S0038094615070199 doi: 10.1134/S0038094615070199

- 956 Vandaele, A. C., Korabiev, O., Daerden, F., Aoki, S., Thomas, I. R., Altieri, F., ...
 957 Zorzano, M. (2019, Apr). Martian dust storm impact on atmospheric H₂O and
 958 D/H observed by ExoMars Trace Gas Orbiter. *Nature*, *568*(7753), 521-525.
 959 doi: 10.1038/s41586-019-1097-3
- 960 Vandaele, A. C., Lopez-Moreno, J.-J., Patel, M. R., Bellucci, G., Daerden, F., Ristic,
 961 B., ... the NOMAD Team (2018, Jun 19). Nomad, an integrated suite of
 962 three spectrometers for the exomars trace gas mission: Technical description,
 963 science objectives and expected performance. *Space Science Reviews*, *214*(5),
 964 80. Retrieved from <https://doi.org/10.1007/s11214-018-0517-2> doi:
 965 10.1007/s11214-018-0517-2
- 966 Veyret, B., Rayez, J. C., & Lesclaux, R. (1982). Mechanism of the photooxidation of
 967 formaldehyde studied by flash photolysis of formaldehyde-oxygen-nitric oxide
 968 mixtures. *The Journal of Physical Chemistry*, *86*(17), 3424-3430.
- 969 Villanueva, G., Mumma, M., Novak, R., Radeva, Y., Kufl, H., Smette, A., ...
 970 Hartogh, P. (2013). A sensitive search for organics (ch₄, ch₃oh, h₂co,
 971 c₂h₆, c₂h₂, c₂h₄), hydroperoxyl (ho₂), nitrogen compounds (n₂o, nh₃,
 972 hcn) and chlorine species (hcl, ch₃cl) on mars using ground-based high-
 973 resolution infrared spectroscopy. *Icarus*, *223*(1), 11 - 27. Retrieved from
 974 <http://www.sciencedirect.com/science/article/pii/S0019103512004599>
 975 doi: <https://doi.org/10.1016/j.icarus.2012.11.013>
- 976 Webster, C. R., Mahaffy, P. R., Atreya, S. K., Flesch, G. J., & Farley, K. A. (2013).
 977 Low upper limit to methane abundance on mars. *Science*, *342*(6156), 355-357.
 978 Retrieved from <https://science.sciencemag.org/content/342/6156/355>
 979 doi: 10.1126/science.1242902
- 980 Webster, C. R., Mahaffy, P. R., Atreya, S. K., Flesch, G. J., Mischna, M. A.,
 981 Meslin, P. Y., ... Lemmon, M. T. (2015). Mars methane detection
 982 and variability at gale crater. *Science*, *347*(6220), 415-417. Retrieved
 983 from <http://science.sciencemag.org/content/347/6220/415> doi:
 984 10.1126/science.1261713
- 985 Webster, C. R., Mahaffy, P. R., Atreya, S. K., Moores, J. E., Flesch, G. J., Male-
 986 spin, C., ... Vasavada, A. R. (2018). Background levels of methane in mars'
 987 atmosphere show strong seasonal variations. *Science*, *360*(6393), 1093-1096.
 988 Retrieved from <http://science.sciencemag.org/content/360/6393/1093>
 989 doi: 10.1126/science.aaq0131
- 990 Wong, A. S., & Atreya, S. K. (2004). Atmospheric photochemistry above possible
 991 martian hot spots. *Advances in Space Research*, *33*(12), 2236 - 2239.
 992 Retrieved from [http://www.sciencedirect.com/science/article/pii/](http://www.sciencedirect.com/science/article/pii/S0273117703005246)
 993 [S0273117703005246](http://www.sciencedirect.com/science/article/pii/S0273117703005246) (Mercury, Mars and Saturn) doi: [https://doi.org/](https://doi.org/10.1016/S0273-1177(03)00524-6)
 994 [10.1016/S0273-1177\(03\)00524-6](https://doi.org/10.1016/S0273-1177(03)00524-6)
- 995 Wong, A.-S., Atreya, S. K., & Encrenaz, T. (2003). Chemical markers of possible
 996 hot spots on mars. *Journal of Geophysical Research: Planets*, *108*(E4).
 997 Retrieved from [https://agupubs.onlinelibrary.wiley.com/doi/abs/](https://agupubs.onlinelibrary.wiley.com/doi/abs/10.1029/2002JE002003)
 998 [10.1029/2002JE002003](https://doi.org/10.1029/2002JE002003) doi: 10.1029/2002JE002003
- 999 Zahnle, K., Freedman, R. S., & Catling, D. C. (2011). Is there methane on mars?
 1000 *Icarus*, *212*(2), 493 - 503. Retrieved from [http://www.sciencedirect.com/](http://www.sciencedirect.com/science/article/pii/S001910351000446X)
 1001 [science/article/pii/S001910351000446X](http://www.sciencedirect.com/science/article/pii/S001910351000446X) doi: [https://doi.org/10.1016/](https://doi.org/10.1016/j.icarus.2010.11.027)
 1002 [j.icarus.2010.11.027](https://doi.org/10.1016/j.icarus.2010.11.027)